 doi:10.20944/preprints202011.0030.v1

Article

Mapping of the Canopy Openings in Mixed Beech-Fir Forest at Sentinel-2 Subpixel level Using UAV and Machine Learning Approach

Ivan Pilaš [1,*], Mateo Gašparović [2], Alan Novkinić [3] and Damir Klobučar [4]

[1] Croatian Forest Research Institute, Division of Ecology, Cvjetno naselje 41, 10450, Jastrebarsko, Croatia; ivanp@sumins.hr
[2] Faculty of Geodesy, University of Zagreb, Department of Photogrammetry and Remote Sensing, Kačićeva 26, 10000 Zagreb, Croatia; mateo.gasparovic@geof.unizg.hr
[3] Croatian Forests Ltd., Ivana Meštrovića 28, 48000 Koprivnica, Croatia; alan.novkinic@hrsume.hr
[4] Croatian Forests Ltd., Ivana Meštrovića 28, 48000 Koprivnica, Croatia; damir.klobucar@hrsume.hr
* Correspondence: ivanp@sumins.hr; Tel.: +385-98-326-714

Abstract: The presented study demonstrates the bi-sensor approach suitable for rapid and precise up-to-date mapping of forest canopy gaps for the larger spatial extent. The approach makes use of UAV RGB images on smaller areas for highly precise forest canopy mask creation. Sentinel-2 was used as a scaling platform for transferring information from UAV to a wider spatial extent. The various approaches of the improvement of the predictive performance were examined: (I) the highest R2 of the single satellite index was up to 0.57, (II) the highest R2 using multiple features obtained from the single date, S-2 image was 0.624 and, (III) the highest R2 on the multi-temporal set of S-2 images, was 0.697. Satellite indices such as ARVI, IPVI, NDI45, PSSRa, MCARI, CI, RI, and NDTI were the dominant predictors in most of the ML algorithms. The more complex ML algorithms such as SVM, Random Forest, GBM, XGBoost, and Catboost that provided the best performance on the training set exhibited weaker generalization capabilities. Therefore, a simpler and more robust Elastic Net algorithm was chosen for the final map creation.

Keywords: Sentinel-2; UAV; machine learning; forest canopy; canopy gaps; canopy openings percentage; satellite indices; Elastic Net; beech-fir forests

1. Introduction

Forest canopy gaps, as a consequence of management activities or natural disturbances, are the main drivers that affect the forest dynamics in most of the continuous cover, Close-to-Nature silvicultural systems. Gap-based interventions to create a more open stand structure is one of the most common silvicultural practices for regeneration, as well as forest exploitation in the mixed silver fir (Abies alba Mill.) and European beech (Fagus sylvatica L.) forests in Central Europe. The size and position of crown openings determine the amount of direct light able to penetrate to the forest floor, thus creating conditions that could favour the shade-tolerant silver fir or the regeneration of the more competitive European beech in conditions of supplementary light availability [1]. The creation of treefall-gaps accelerates tree regeneration and increases tree species diversity in mixed beech – fir forests [2]. The creation of canopy openings through natural tree mortality processes, wind-driven gap formation, or man-made activities also has a significant influence on changes in microclimatic conditions and below-ground processes. Canopy openings have an impact on increases in air and soil temperatures and decreases in soil moisture in larger gaps [3]. Humification processes prevail in small gaps i.e. an increase in soil organic content while in large gaps the mineralization processes related to decreases in organic content are more dominant [4,5]. The questions of size, shape, and topographic position of forest openings have been extensively studied [6-13]. They have been done so as to emulate the natural disturbance processes and to discover the most appropriate silvicultural

 doi:10.20944/preprints202011.0030.v1

operations that would imitate natural regeneration, in particular with the aim of conversion of various monocultures towards Close-to-Nature forests [14].

The estimation of the forest canopy gaps or openings is commonly obtained from measures of canopy cover that can be defined as a percentage of forest area occupied by the vertical projection of tree crowns, unlike the canopy closure that has an analogous meaning but is represented by the proportion of sky hemisphere obscured by vegetation when viewed from a single point. There are three different groups of approaches [15] for measuring or estimating the crown canopy density in a forest: (I) ground measurement at the study area, (II) statistical approaches, if the information such as basal area or DBH and the number of stems is available, (III) remote sensing data such as aerial photographs, satellite data or laser scanner data. When making ground measurements, devices such as densiometers and hemispherical digital photographs are used or they are based on pure ocular assessment [16,17]. These methods are labour intensive and cannot quickly provide accurate canopy cover estimates [17]. Recently, remote sensing methods, in particular Light Detection and Ranging (LiDAR), have been proven as the most advantageous approaches in terms of accuracy and cost efficiency [18-21]. UAV (Unmanned Aerial Vehicle) based LiDAR has a lower cost, more convenient operation and more flexible flight route design than airborne LiDAR, as well as unique advantages in the high-precision acquisition of high-density point clouds [19]. Satellite remote sensing, medium resolution data from Landsat, is traditionally a very appropriate source of information for crown cover estimation, most often comprising the supervised classification approaches based on ground truth validation sets obtained from field measurements, airborne or UAV aero photo imagery, LiDAR or very high-resolution satellite imagery [22-28]. The main drawback of the medium resolution satellite data such as Landsat 8 is that its spatial resolution of 30 m is too coarse for precise forest gaps detection. One of the most prominent examples of canopy closure estimation worth mentioning is Tree cover density product in 20 m resolution, developed for the Pan-European scale in 2012, 2015, 2018, as part of the Copernicus Land Monitoring Service [29].

By launching a pair of Sentinel-2 satellites in 2015 and 2017, the European Space Agency – ESA made a considerable breakthrough in improving the ability of the global monitoring of conditions and changes in forest cover primarily due to cost-free data availability, as well as highly advanced sensor characteristics: very good spectral properties (13 bands from 492.1 to 2185.7 nm, central wavelengths), radiometric resolution (12 bit; a potential range of brightness levels from 0 - 4 095), spatial resolution (10 m of RGB and NIR bands) and revisit time (5 days under cloud-free conditions) [30]. These characteristics enable improved monitoring of the conditions and changes in the land cover and its dynamics on a global scale. Sentinel 2 MSI with a 10 meter spatial resolution shows some improvement in the possibility of detection of selective logging gaps in relation to Landsat 8 [31, 32, 33]. On the other hand, the possibilities of the employment of Sentinel 2 in operational forestry to its full performance have not been fully recognized and valorised up to the present. Apparently, a major disadvantage of the Sentinel 2 MSI sensor, which limits its greater use in forestry, is its 10-meter spatial resolution which prevents exact geolocation and delineation of individual trees, which is important for many silvicultural practices, and for this reason other more precise survey methods such as LiDAR, UAV images, and VHR satellite imagery are often more attractive and competitive. Finer spatial resolution is especially important in the management of uneven-aged mixed forests where silvicultural interventions take place at the level of an individual tree or a smaller group of trees and we rarely find larger interrupted areas (except in the case of natural disasters such as windbreaks or ice breaks) that could be clearly identified on satellite Sentinel 2 or Landsat 8 images [34].

For the successful implementation of remote sensing products in operational forestry, several prerequisites need to be met, related to their compliance on the scale of which the various forest management planning activities are carried out. Given the temporal scale, we can usually distinguish medium-term forest management planning, usually on a decadal time-scale, based on the conducted forest inventory. In addition, there is more operational, annual planning that requires more current, timely information from the forests based on which operational silvicultural decisions are implemented in the short term. In the case of continuous cover mixed forests, it is of great importance

 doi:10.20944/preprints202011.0030.v1

to mark locations within the forest stand with overly dense canopy structure where a selective cut for regeneration purposes or thinning should be carried out. Further, information on the location of newly created forest gaps, after a natural disaster, windbreak, ice breakage, or biotic damages can be used in the planning of the restoration of these areas, construction of the logging trails, calculation of the man-hours of the forest workers and machines, etc. Regarding the spatial scale, the extent of the supporting data layer should comply with the extent of the forest area that is considered in the operational planning, usually on the scale of the forest managerial unit. In Croatia, with the usual size being between 3000 and 6000 hectares, the forest managerial units (FMU) are the lowest organizational tiers, usually consisting of forest areas with similar characteristics, for which forest management plans (every ten years) and yearly operational plans that more precisely define required silvicultural, forest protection, timber extraction, and other related activities, are conducted. Given the above prerequisites (timeliness, spatial extent, precision), it is unlikely that a single remote sensing source alone is suitable for providing information about the actual state of the forest canopy, the location of the canopy openings i.e. stand density, to be suitable for cost-efficient, operative applications in forestry. Airborne LiDAR and aerial photos (visible and multispectral) can provide high precision information about the crown surface; however, they are relatively expensive surveys and are more often used for cyclical inventories (every ten years). UAV presents a more practical solution to an airborne survey; however, a large spatial extent (3000-6000 hectares) of the FMU often represents a limitation for its operational use where the maximal daily UAV survey limit is up to 400 hectares. Very high-resolution satellite data fulfils the requirements of spatial extent and timeliness but can be very expensive for everyday operational use. On the other hand, the cost-free Sentinel 2 data has the constraints of insufficient resolution for precise forest canopy gap detection.

This study aims to evaluate the novel, cost-efficient approach of precise mapping of the current, actual state of the forest Canopy Openings Percentage (COP) suitable for the silvicultural decision-making process in forest management on an intra-annual operational scale. It is based on the bi-sensor approach; it takes advantage of the Sentinel 2 as an auxiliary source of information, very suitable for the large-scale mapping, and derived high-precision forest mask from the UAV imagery as ground truth, obtained on pre-defined training/validation locations inside FMU consisting of the mixed beech-fir forest. This approach of integration of the Sentinel-2 and UAV has been recently broadly implemented in various domains; in forestry, to estimate the aboveground biomass of Mangrove plantations [35], in agriculture to estimate rice crop damages [36] and for water quality monitoring [37]. This study aims to improve the spatial precision of the Sentinel-2, using its enhanced spectral properties that are suitable for capturing and quantifying the very fine shifts in the forest canopy cover at a subpixel level. This is provided by using a standard machine-learning framework that consists of the features engineering, training and validation set creation, machine learning algorithms examination and validation by fine-tuning, selection of the final model, and final map creation. In this predictive modelling framework, the specific objectives of the research that are closely related to the improvement of the predictive capabilities and performance of the models emerge; (I) the suitability of single-source Sentinel-2 image versus the multitemporal set of Sentinel-2 images, closest as possible to the date of UAV image acquisition, (II) the predictive power of the various satellite indices i.e. spectral features, (III) the most suitable machine learning algorithm among existing ones, having in mind the predictive performance and overfitting.

2. Materials and Methods

2.1. Study area

The study area is located in the north-eastern, continental part of the Dinaric Alps, a massif in southern and south-eastern Europe which stretches for 645 kilometers and separates the continental area of the Balkan Peninsula from the Adriatic Sea. The exact location (Figure 1) is near the town of Vrbovsko, Gorski Kotar region, Croatia (45.4282 Latitude and 15.0714 Longitude). The research covered the Litorić forest managerial unit (FMU), with an area of 3181.82 hectares, which administratively belongs to the Vrbovsko Forest Office, Forest District Delnice, as an integral part of the state-owned

Preprints (www.preprints.org) | NOT PEER-REVIEWED | Posted: 2 November 2020 doi:10.20944/preprints202011.0030.v1

forests managed by the Croatian Forests state company. The FMU Litorić is located in an altitude range of 400 to 900 meters and it has 91 compartments. The total wood stock is 965,636 m³ (313 m³ / ha), and the total annual increment is 202,015 m³ (6.5 m³ / ha). FMU Litorić consists of 35.45% of common beech with 342,297 m³ of wood stock and 50.11% of common fir with stocks of 483,894 m³. In terms of other species, there are also 8.78% mountain maple, 2.88% spruce and other hardwoods. According to vegetation typology, the research area is part of a very broad range of European mountain beech forests, subgroup of Illyrian mountainous beech forests [38] of the Dinaric Alps, where the common beech occurs in combination with the common fir and forms special mixed vegetation forests with high biodiversity and economic value. The lithological base is predominantly composed of limestone and dolomite with associated brown soils.

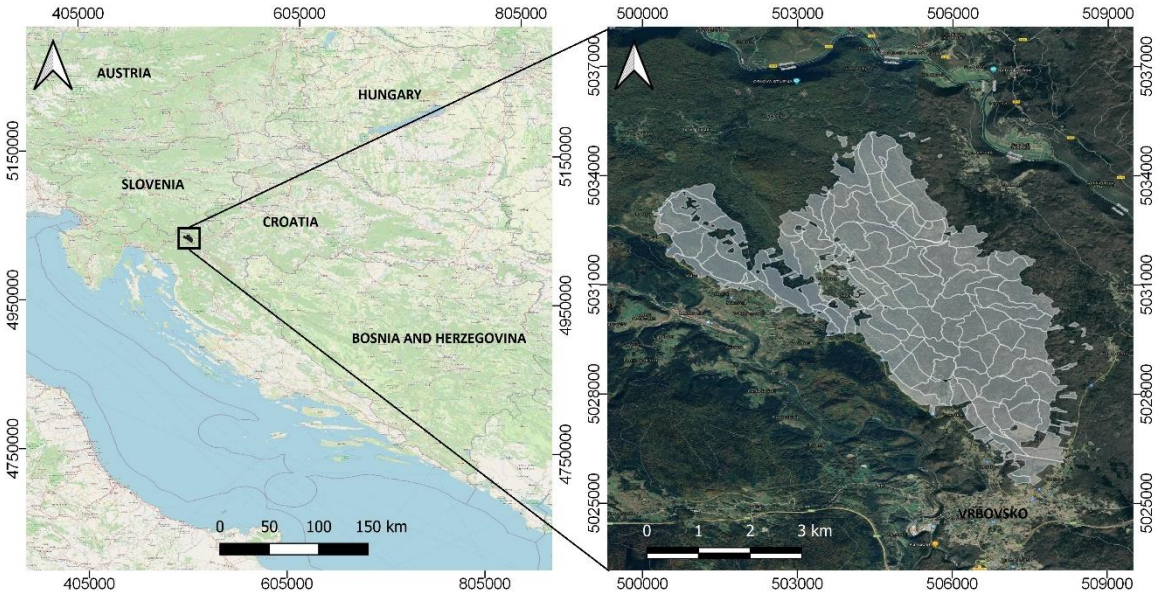

Figure 1. The location of the study area, Forest Management Unit "Litorić"

From the perspective of the prevailing end-users in the area, forest managers in the past decade have mostly been concerned about increases in biotic and abiotic damage. Forests in FMU have been influenced by a prolonged outbreak of spruce bark beetle (Pityokteines curvidens) which causes a weakening of the vitality of trees and forest stands with the occurrence of occasional individual and group dieback of trees. Besides this, most likely as a consequence of climate change, very fierce storms with strong winds have appeared in the last few years causing windbreaks and windthrows. The storm that took place at the beginning of November 2017, followed by a few strong wind events in 2018, had a particularly strong impact in terms of the spatial extent of forest damage. During these incidents, mostly fir trees were damaged due to the resistance provided by their canopy, while beech trees were damaged to a much lesser extent. Considering that classical terrestrial methods of observation could not accurately determine the spatial effect of wind damage, subsequent log hauling, and surface remediation for the scale of the whole FMU, the COP estimation method was approached by combined remote sensing means and methodology presented in this study.

2.2. UAV survey of the training and the testing area

A detailed survey of the parts of the FMU Litorić using UAV was performed at the end of July 2018. The survey included two independent locations, one of which, with a size of 470 hectares, was selected as a training area, and the other, with a size of 310 hectares as a testing area for selected modelling algorithms (Figure 2). The images in the visible RGB channel were taken using a DJI INSPIRE 2 drone with a ZENMUSE X5S camera with gyroscopic stabilization at a height of 300 meters from the

Preprints (www.preprints.org) | NOT PEER-REVIEWED | Posted: 2 November 2020 doi:10.20944/preprints202011.0030.v1

ground. All recorded material was transformed in the WGS84 coordinate system. Esri Drone2Map software was used for photo processing and DOF creation, while cartographic processing was done in the ArcMap 10.6.1. program. The final product presents ortho-rectified high precision images of the parts of FMU with a spatial grid resolution of 7 cm, based on which highly precise canopy boundaries could be delineated and masked out in further processing.

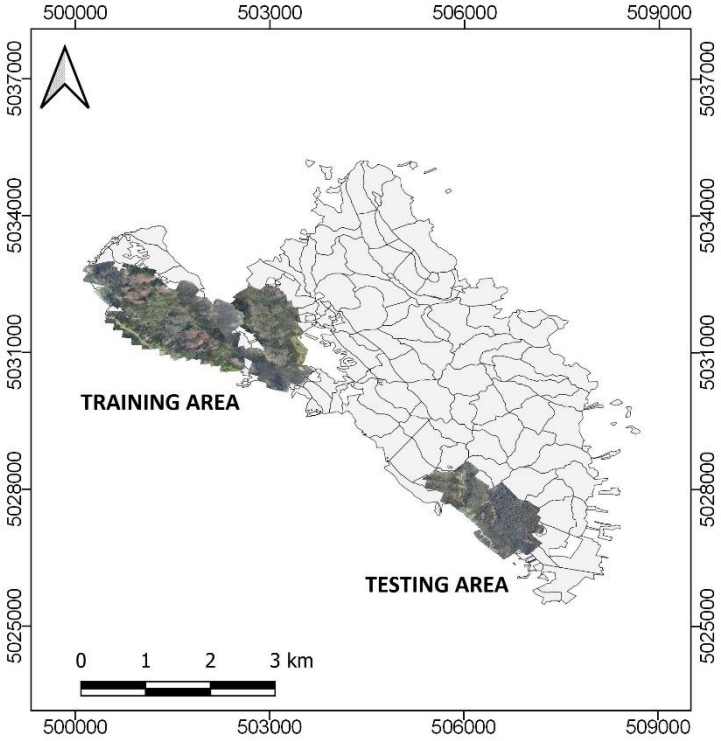

Figure 2. The locations of training and testing areas

2.3. Satellite image processing and indices extraction

For this study, 4 Sentinel-2 Level 2A (S2_L2A) cloud-free, Bottom Of Atmosphere reflectance products were used which consisted of 100 km by 100 km squared ortho-images in UTM/WGS84 projection. Cloud free imagery, temporarily consistent as much as possible with performed UAV surveys (within a approx. 2-month period) were selected and retrieved from the Copernicus Open Access Hub [38]. Also, all four S2_L2A images have an almost identical time of acquisition and relative orbit position (Table 1). For the purpose of analysis, no additional image enhancement processing of S2_L2A was performed. After the acquisition, due to the differences in pixel resolution, all S2_L2A bands were resampled to a 10 m extent using default resampling processor parameters in the Sentinel Application Platform (SNAP), cost-free software provided by the European Space Agency (ESA). Prior to further analysis, the collocation of images was performed i.e. pixel values of S2_L2A images were resampled into the geographical raster of the master image from 25.7.2018.

Table 1. Details of Sentinel 2 Level 2A products used in this study

Platform ID	Year	Month	Day	Time of acquisition	Relative orbit number	Tile number field
S2A	2018	7	25	10:00	R122	T33TVL
S2B	2018	8	1	10:00	R122	T33TVL
S2B	2018	8	29	10:00	R122	T33TVL
S2B	2018	9	28	10:00	R122	T33TVL

 doi:10.20944/preprints202011.0030.v1

The Sentinel 2 multi-spectral instrument (MSI) has 13 spectral channels in the visible/near-infrared (VNIR) and short wave infrared spectral range (SWIR) that facilitate the possibility of the construction of a wide range of spectral indices. The development of satellite platforms and sensors over the past decades have also been accompanied by an intensive contrivance of various satellite indices aimed at better discrimination of land surface categories and objects [39]. The fundamental principle of the differentiation of vegetation cover on multispectral images is based on the ratio between the red part of the spectrum that is absorbed by the chlorophyll in the leaves and the infra-red part of the spectrum that is reflected by vegetation. Vegetation indices were developed with the intention of clearer quantification of the intensity of vegetation activity with the best possible reduction of accompanying noise. Noise that exists in satellite images and derived indices is usually a consequence of topography, reflection from bare soil, soil color, atmosphere, spectral characteristics of sensors, view, and solar zenith angels [40].

Depending on the approach of noise separation, especially soil line differentiation, vegetation indices are further divided into slope-based, distance-based, and orthogonal [41]. In contrast to a wide range of vegetation indices, soil radiometric indices were primarily developed with the aim of more complete quantification of soil optical properties. Primarily, this refers to the determination of different degrees of soil brightness as a result of viewing geometry, the surface roughness, the organic matter, water contents, and spectral features occurring in the visible domain i.e. soil color [42]. The more intrinsic insight into the structure and photosynthetic processes of vegetation provide biophysical variables such as LAI, FAPAR, FVC, CAB, CWC that present a proxy for the estimation of canopy cover, photosynthetic dynamics, leaf water content and can be effectively derived from Sentinel 2 bands [43]. A special group of features, developed from digital image analysis, is based on the detection and quantification of gray textures and tones in the images. This can significantly improve the separation of objects and structures in images and are also very suitable for use in various machine learning methods [44].

Considering very heterogeneous surface conditions in the study area of FMU Litorić with various possible spectral feedbacks (areas of undisturbed mixed species canopy, fragments of bare soil surface after logging, open forest gaps with understory shroud of plants and shrubs, occasional groups of sprawled trees, etc.), it was necessarily to use a broader variety of spectral indices. Furthermore, the statistical and machine learning methods can quite successfully isolate the contribution of individual input features on the final predictive outcome. Therefore, various groups of spectral indices such as vegetation indices, soil reflection indices, biophysical variables, and textural properties (Gray level co-occurrence matrix) were used in this study (Table 2). The selection of the applied indices depended on the pre-defined catalogue of indices that can be automatically retrieved through an in-built S-2 index processor in SNAP software. For each of the considered satellite images, (S2_20180725, S2_20180801, S2_20180829, S2_20180928) a total of 155 predictors were calculated.

Table 2. Derived satellite indices and textural features

Satellite Index	Spectral bands	Sentinel 2 bands
Soil radiometric indices		
BI - Brightness Index	red, green	B4, B3
BI2 - The second brightness image	red, green, NIR	B4, B3, B8
RI - Redness Index	red, green	B4, B3
CI - Colour Index	red, green	B4, B3
Vegetation radiometric indices		
SAVI - Soil Adjusted Vegetation Index	red, NIR	B4, B8
NDVI - Normalized Difference Vegetation Indeks	red, NIR	B4, B8
TSAVI - Transformed Soil Adjusted Vegetation Index	red, NIR	B4, B8
MSAVI - Modified Soil Adjusted Vegetation Index	red, NIR	B4, B8
MSAVI2 - The second Modified Soil Adjusted Vegetation Index	red, NIR	B4, B8

 doi:10.20944/preprints202011.0030.v1

DVI - Difference Vegetation Indeks	red, NIR	B4, B8
RVI - Ratio Vegetation Index	red, NIR	B4, B8
PVI - Perpendicular Vegertation Index	red, NIR	B4, B8
IPVI - Infrared Percentage Vegetation Index	red, NIR	B4, B8
WDVI - Weighted Difference Vegetation Index	red, NIR	B4, B8
TNDVI - Transformed Normalized Difference Vegetation Index	red, NIR	B4, B8
GNDVI - Green Normalized Difference Vegetation Index	green, NIR	B3, B7
GEMI - Global Environmental Monitoring Index	red, NIR	B4, B8A
ARVI - Atmospherically Resistant Vegetation Index	red, blue, NIR	B4, B2, B8
NDI45 - Normalized Difference Index	red, red edge	B4, B5
MTCI - Meris Terrestrial Chlorophyll Index	red, red edge, NIR	B4, B5, B6
MCARI - Modified Chlorophyll Absorption Ratio Index	red, red edge, green	B4, B5, B3
REIP - Red Edge Inflection Point Index	red, red edge, red edge, NIR	B4, B5, B6, B7
S2REP - Red Edge Position Index	red, red edge, red edge, NIR	B4, B5, B6, B7
IRECI - Inverted Red Edge Chlorophyll Index	red, red edge, red edge, NIR	B4, B5, B6, B7
PSSRa - Pigment Specific Simple Ratio Index	red, NIR	B4, B7
Water Radiometric Indices		
NDWI - Normalized Difference Water Index	NIR, MIR	B8, B12
NDWI2 - Second Normalized Difference Water Index	green, NIR	B3, B8
MNDWI - Modified Normalized Difference Water Index	green, MIR	B3, B12
NDPI - Normalized Difference Pond Index	green, MIR	B3, B12
NDTI - Normalized Difference Turbidity Index	red, green	B4, B3
Biophysical indices		
LAI - Leaf Area Index		B3, B4, B5, B6, B7, B8a, B11,
FAPAR - Fraction of Absorbed Photosynthetically Active Radiation		B12, cos(viewing_zenith),
FVC - Fraction of Vegetation Cover		cos(sun_zenith),
CAB - Chlorophyll Content in the Leaf		cos(sun_zenith),
CWC - Canopy Water Content		cos(relative_azimuth_angle)
Texture (Grey Level Co-occurance Matrix)		
Contrast		
Dissimilarity		
Homogeneity		
Angular Second Moment		
Energy		
Maximum Probability		
Entropy		
GLCM Mean		
GLCM Variance		
CLCM Correlation		

 doi:10.20944/preprints202011.0030.v1

2.4. Integration of Sentinel 2 and UAV data

One of the fundamental challenges in this research was the integration of satellite S2_L2A and photogrammetric UAV images on the same spatial scale. The S2_L2A multispectral product consists of bands with a spatial resolution of 10 m (band 2, band 3, band 4, and band 8), 20 meters (band 5, band 6, band 7, band 11, and band 12), and 60 meters (band 1, band 9 and band 10). Before further processing, all bands were rescaled to a 10 meter resolution which is a routine procedure in software such as SNAP. All S2_L2A multi-temporal products were also collocated on the same spatial grid. The spatial resolution of the UAV images was approximately 7 cm, i.e. 143 times finer than the S2_L2A so that one Sentinel pixel of 10x10m contains 20 449 UAV pixels. Although there are available analytical tools that allow rescaling raster images to finer spatial resolution, such processing methods, due to extremely large differences in spatial resolutions of the imagery, were not suitable because they require high-performance computing capabilities and long-term computer processing time. Also, the use of R analytical tools in this research, with exceptional capabilities for statistical or machine learning processing, required rearrangement of input spatial data in the standardized R form (a form of matrix or data frame). In that sense, preparation and aggregation of data followed the principles of "tidy" data standardization described by [46], who defines tidy data as follows: each variable forms a column, each observation forms a row and each type of observational unit forms a table.

Before data aggregation, canopy boundaries were extracted from RGB UAV bands, and a canopy mask layer was created. Acquired aerial imagery was processed similarly to the methodology presented in the research [47]. A generated high-resolution digital orthophoto was used to create various spectral indices that were tested for fast and accurate canopy mask layer creation. In accordance with the [48] the best spectral indices were chosen. Although many indices were tested, such as Brightness Index (BI)[49]; Redness Index (RI)[50], Colour Index (CI)[51], Green Leaf Index (GLI)[52], Normalized Green Red Difference Index (NGRDI)[53], Visual Atmospheric Resistance Index (VARI)[54], just three of them were selected: NGRDI, VARI, and GLI. Namely, the mentioned indices mostly distinguish the healthy forest from bare land, windthrows, or canopy openings. The high-resolution UAV-based canopy mask layer was created using the R program language.

The percentage of canopy density for every S2_L2A pixel overlaying the UAV imagery was made by first producing an S2_L2A fishnet grid with a cell size of 10x10 m. Since all S2_L2A images were collocated and resampled, the derived fishnet grid was used on all multi-temporal imagery sets. The fishnet grid was then overlapped with regular points i.e., 10 x 10 points (100 points per S2_L2A grid cell). A sampling of the UAV images was performed according to binary outcomes so that the values of the mask layer (forest canopy) were marked as 0 while the areas outside the canopy (forest gaps) were marked as binary 1. The percentage (COP) for each of the S2_L2A pixels was obtained from the ratio of the sum of 1 (outside the canopy mask) and the total number of points (100) in each grid cell. Then, for each S2_L2A polygon in the fishnet, a centroid was calculated to which the COP value was assigned as a percentage so that each of the pixels on the satellite image was represented with only one point and the corresponding COP value. Further preparation included a random sampling of 10% points on the S2_L2A polygon grid to minimize the effect of spatial correlation between the sampling points on the images. At each selected random centroid or point, sampling of derived satellite indices was performed on multi-temporal imagery. After preparation and sampling, all the data was compiled into data frames; a training data frame with 4653 observations and 155 predictor variables for a single S2_L2A image and 620 predictors for the entire multitemporal set). The test set consisted of an equal number of input variables and 3596 observations.

2.5. Model building and validation

Various statistical and machine learning (ML) algorithms of different levels of complexity were examined for the prediction and mapping of the COP. The construction of the models was performed on the training set of observations, retrieved from the selected UAV training area. The performance of

Preprints (www.preprints.org) | NOT PEER-REVIEWED | Posted: 2 November 2020 doi:10.20944/preprints202011.0030.v1

different algorithms was examined on the training set across the range of fine-tuning parameters using the 10-fold cross-validation (CV) resampling method and standard metrics that are used in regression analysis: Root Mean Square Error (RMSE) and the coefficient of determination (R^2). The 10-fold cross-validation technique that was used concerning other resampling methods gives the best estimate of the actual RMSE and the most favorable trade-off between the bias and variance of the model (Kuhn and Johnson 2013). All models were also validated on the test set from the physically separate UAV survey area to examine the effect of the spatial extrapolation, using the selected model out of the training area. The procedure of the model construction was repeated twice: the first time using only predictors from the single date S2_L2A image from 2018/07/25 and the second time using a multitemporal set of the four S2_L2A images, with close dates of acquisition (2018/07/25, 2018/08/01, 08/29/2018, 09/28/2018). As previously mentioned, the response variable is the COP percentage on the interval quantitative scale (full canopy = 0 % - open ground = 100%). All computation was performed in the generic R modelling package Caret, which has the possibility of pre-processing input data, training, testing, and precise adjustment of a large number of statistical and machine learning algorithms [55]. In the R Caret modelling interface, a suitable R package was additionally installed for each of the considered algorithms: *stats* package for Ordinary Least Squares, *pls* package for Partial Least Squares, *elasticnet* package for Ridge Regression and Elastic Net, *nnet* package for Neural Networks, *e1071* package for Support Vector Machines, *randomForest* package for Random Forest, *gbm* package for Stochastic Gradient Boosting, *xgboost* for Extreme Gradient Boosting and *catboost* package for CatBoost algorithm.

2.5.1. Ordinary least squares (OLS) linear regression

The OLS linear regression method has been used as a benchmark model, the results of which served for comparison with other more complex algorithms. Before OLS construction, training data was pre-processed using centring and scaling of predictor variables (zero mean and standard deviation of one). Improvements in the fit by decorrelation and reduction of predictors set using Principal Component Analysis (PCA) and fitting of the PCA components in the OLS model was also examined. OLS, in short, minimizes the sum-of-squared errors (SSE) between the observed and predicted response, the parameter estimates that minimized SSE are the ones that have the least bias. OLS is a very attractive technique with regards to the interpretability of the coefficients but has a drawback in that it is sensitive to the collinearity among predictors and is not suitable when the data has a curvature or nonlinear structure.

2.5.2. Partial Least Squares (PLS)

The PLS method is a very suitable technique in the case of high correlation among predictors where OLS is unstable and not appropriate. The principle behind PLS is that it finds the linear combinations of predictors, called components or latent variables, that maximally summarize the variation in the predictor space. Besides this, the determined components have a maximum correlation with the response. PLS has one tuning parameter, the number of components to retain.

2.5.3. Ridge Regression (RR)

Ridge Regression is a linear regularization method suitable where there are issues with collinearity and in cases of the overfitting of the data. It belongs to a group of shrinkage methods that adds penalties or shrinks the parameter estimates which do not contribute significantly to the reduction of the SSE. In the bias-variance trade-off, Ridge regression reduces the Mean Square Error by slightly increasing the bias by adding appropriate penalties. The penalty presents a tuning parameter that was optimized by cross-validation during the model training process.

 doi:10.20944/preprints202011.0030.v1

2.5.4. Elastic Net (ENET)

Elastic Net is a linear regularization technique that also effectively deals with high correlated predictors. It combines two different penalties of the Ridge regression and the Lasso model. It is an advancement of the Ridge regression that also makes possible variable selection that is a characteristic of the Lasso model. In the training framework, it is tuned over the various penalty values via cross-validation.

2.5.5. Feed-Forward Neural Networks (NNET)

Neural Networks are nonlinear techniques which use hidden variables or hidden units that present linear combinations of the original predictors. Predictors are transformed by a nonlinear function (logistic, sigmoidal) and each unit is related to the outcome. They are characterized by the large number of estimation parameters which are quite uninterpretable. Due to the large number of the regression coefficients, neural networks have tendency of overfitting. The weight decay is commonly used penalization method that moderates the overfitting problem. In this study, the simplest neural network architecture, a single-layer feed-forward network was used. The tuning parameters used for cross-validation resampling are the number of hidden units and the amount of weight decay.

2.5.6. Support Vector Machines (SVM)

SVM is a non-linear regression and classification technique, that relies on data points (support vectors) above a certain threshold with high residuals. Observations with residuals within the threshold do not contribute to the regression fit i.e. samples that the model fits well have no effect on the regression equation. This makes SVM insensitive to the outliers, very powerful and robust in nature. SVM uses various Kernel functions (linear, polynomial, radial basis) that has the ability to model a nonlinear relationship. SVM tuning parameters are the cost parameter that adjusts the complexity of the model (large cost – more flexible model, small cost – "stiffen" model), the size of the threshold for the selection of the vectors, and the kernel parameter.

2.5.7. Random Forest (RF)

Random Forest is a tree-based regression and classification ensemble technique that significantly improves the performance of tree based methods regarding the reduction of the variance and bias. It uses a random subset of the predictors at each tree split what reduces between trees correlation. The final prediction comprises of average prediction of the models in the ensemble. Models in ensemble form independent "strong learners" that yields an improvement in error rates. RF tuning parameter is the number of randomly selected predictors to choose from at each split.

2.5.8. Boosting (GBM, XGBoost, Catboost)

Boosting presents a group of powerful prediction tools, recently usually outperforming any individual model. The gradient boosting approach relies on the single tree as a base learner and the addition of the "week learners" which are gradually included in the residuals. The current model is added to the previous model, and the procedure continues for a user-specified number of iterations. When the regression tree is used as the base learner, simple gradient boosting for regression has two tuning parameters: tree depth and the number of iterations. Boosting techniques are very popular nowadays and are prone to constant improvements. The classical approach presents a stochastic gradient boosting (GBM) algorithm that uses a random sampling scheme. Recently, there are developed improved approaches such as XGBoost (Extreme Gradient Boosting) and CatBoost. The advantage of XGBoost over traditional GBM is in regularization capabilities and more effective tree pruning. However, the new CatBoost model, with improved capabilities of handling categorical variables and

 doi:10.20944/preprints202011.0030.v1

overfitting show also a significant advantage in the processing speed concerning other boosting methods.

3. Results

3.1. Relationship of UAV Canopy Openings Percentage (COP) and individual Sentinel-2 indices

Prior to starting the modelling process, the relationship between COP and individual S2_L2A indices was assessed. Dependency was firstly visually examined on the scatterplots with LOESS (local regression) smoothing and afterward on simple regression metrics between the COP and the spectral indices. This was performed only on indices from a single S2_L2A 7/25/2018 image which was closest to the date of acquisition of the UAV aero-photo imagery. In Figure 3 that shows scatterplots of selected examples, there is clear evidence of an almost linear negative relationship between COP and the intensity of presented vegetation radiometric indices (NDVI, ARVI, IPVI). Similarly, biophysical indices (FAPAR, LAI) also show a negative relationship in which the nonlinearity between variables is somewhat more pronounced. Soil radiometric indices such as CI and RI show a positive relationship to COP while the relationship between COP and textural features vary to a certain extent from parameter to parameter.

Figure 4 shows S-2 indices sorted by the coefficient of determination (R^2) from the single regression analysis with COP. The best linear relationship with COP ($R^2 = 0.57$) was determined for the ARVI index (Atmospherically Resistant Vegetation Index), then the NDVI (Normalized Difference Vegetation Index; $R^2 = 0.56$) and NDVI derived indices such as IPVI (Infrared Percentage Vegetation Index; $R^2 = 0.56$), TNDVI (Transformed Normalized Difference Vegetation Index; $R^2 = 0.56$) and NDTI ($R^2 = 0.54$). From the so-called soil group of indices, the most significant is CI (Color index; $R^2 = 0.54$), and from the water indices NDTI (Normalized Difference Turbidity Index; $R^2 = 0.54$). Derived biophysical indices such as FAPAR and LAI (Fraction of Adsorbed Photosynthetically Active Radiation; Leaf Area Index) show a slightly weaker linear association with the dependent variable (both $R^2 = 0.44$). Of the textural features, the most significant relationship was found in the GLCM (Gray Level Co-occurrence Matrix) variance and mean in the red, B4 channel ($R^2 = 0.37$, r2 = 0.35).

Preprints (www.preprints.org) | NOT PEER-REVIEWED | Posted: 2 November 2020 doi:10.20944/preprints202011.0030.v1

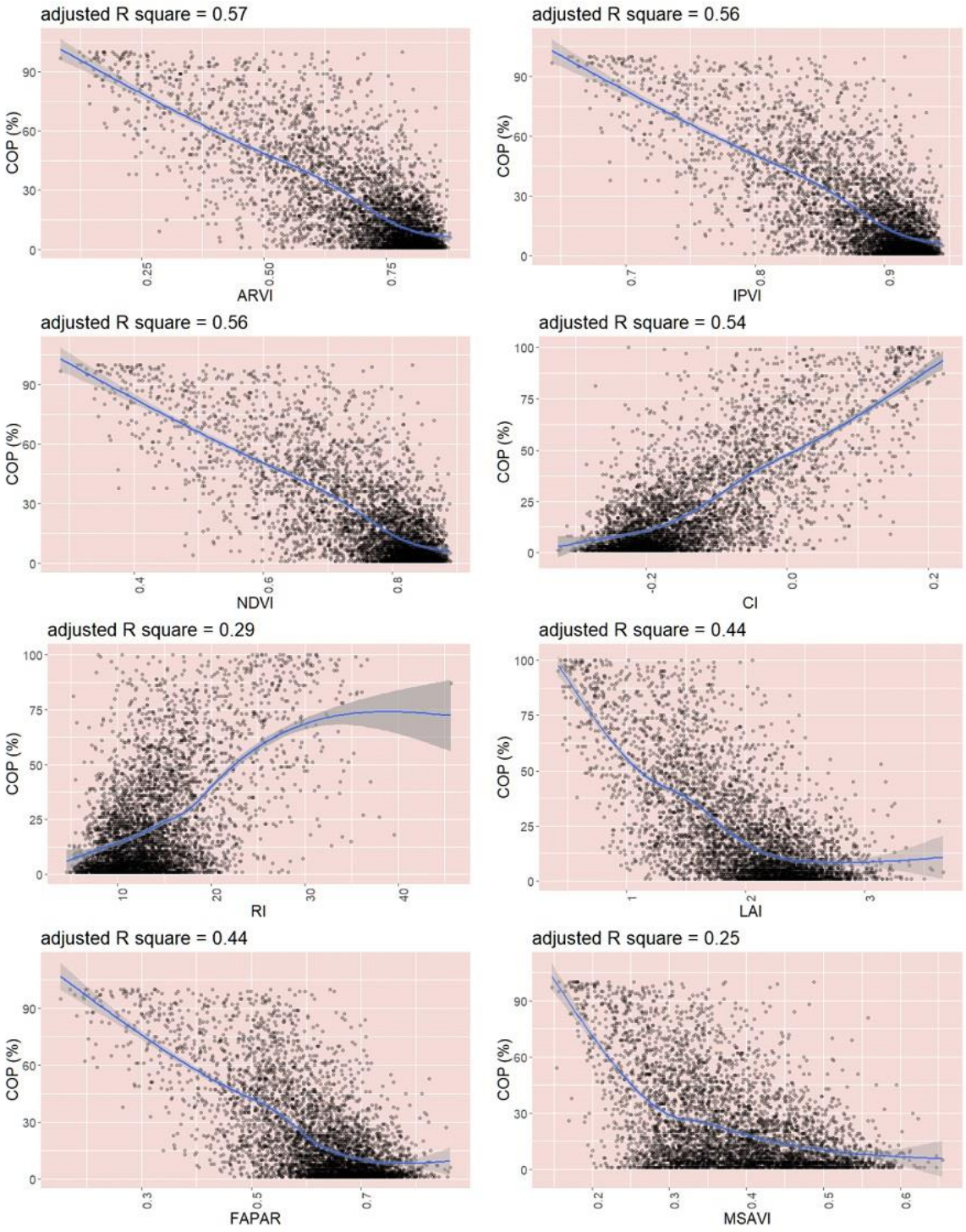

Figure 3. The relationship between individual predictors and COP with included local regression line (Loess)

Preprints (www.preprints.org) | NOT PEER-REVIEWED | Posted: 2 November 2020 doi:10.20944/preprints202011.0030.v1

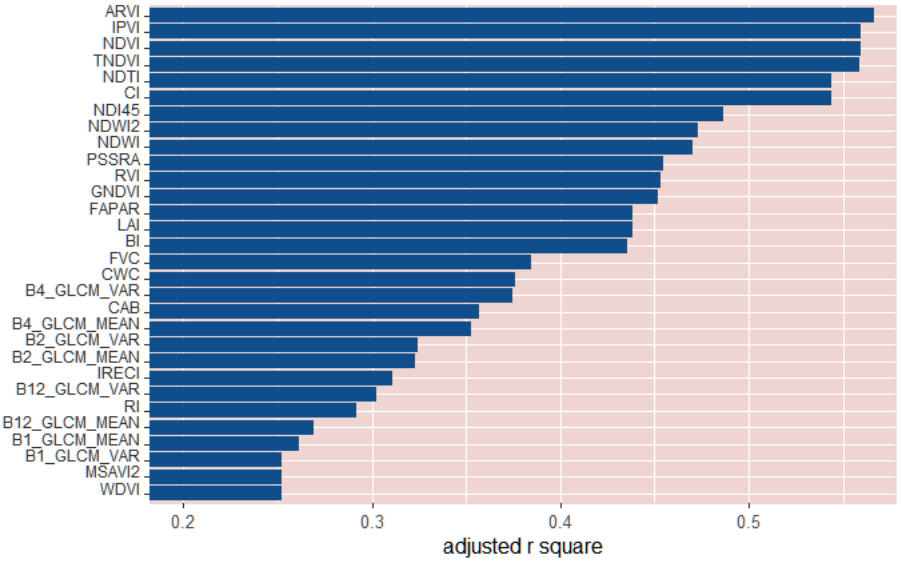

Figure 4. The adjusted coefficient of determination of the 30 most dominant predictors (indices) using simple linear OLS regression

3.2. Training and validation of predictive models

The results of the model training process of COP and indices from single S-2 image from 2018-07-25, using 10-fold CV are presented in Table 3. It shows Root Mean Square Error (RMSE), Coefficient of determination (R^2), Mean Absolute Error (MAE) and final tuning parameters for each selected model obtained by resampling technique. Compared to simple regression results, the inclusion of a multiple set of predictors from a single S-2 image led to an improvement in prediction, but not to a larger extent. The Basic OLS model clearly overfits the data as is noticeable from the decrease of R^2 (from 0.603 to 0.571) when using PCA pre-processing. The addition of other algorithms such as PLS, RR, ENET, NNET, SVM, RF, GBM, XGBoost, Cboost only slightly improve the prediction results. The complex ensemble model such as XGBoost showed the superior results on the training set (R^2=0.624, RMSE= 15.148, MAE=11.070). On the other hand, the highly complex NNET algorithm performs below average (R^2=0.591, RMSE= 15.864, MAE=11.531).

Table 3. The results of 10-fold CV on the training set using single S-2 image

10 fold CV training set - Single Sentinel-2 image (S2 2018-07-25)				
model	**RMSE**	**R^2**	**MAE**	**Tuning parameters**
Multiple regression (Ordinary Least Squares) - OLS	15.684	0.603	11.366	
Multiple regression (Ordinary Least Squares) with PCA pre-processing - OLS with PCA	16.301	0.571	11.909	
Partial Least Squares - PLS	15.618	0.604	11.397	ncomp = 20
Ridge Regression RR	15.611	0.606	11.305	lambda = 0.007142857
Elastic Net - ENET	15.629	0.605	11.314	fraction = 1 lambda = 0.01

Preprints (www.preprints.org) | NOT PEER-REVIEWED | Posted: 2 November 2020 doi:10.20944/preprints202011.0030.v1

Model Averaged Neural Network - NNET	15.864	0.591	11.531	size = 5 decay = 0.01
Support Vector Machines with Radial Basis Function Kernel - SVM	15.344	0.622	10.784	sigma = 0.007735318 C = 2
Random Forest - RF	15.394	0.616	11.374	mtry = 10
Stochastic Gradient Boosting - GBM	15.376	0.616	11.206	n.trees = 910 interaction.depth = 7 shrinkage = 0.01 n.minobsinnode = 20
Extreeme Gradient Boosting - XGBoost	15.148	0.624	11.070	nrounds=550 max_depth=5 eta=0.025
Catboost - Cboost	15.308	0.619	11.197	depth=8 learning_rate=0.1 leaf_reg=0.001 rsm=0.95

Model building on the multi-temporal S-2 data significantly improved prediction results as is obvious from Table 4. The best results on the training set were provided by the SVM algorithm (R^2=0.697, RMSE= 13.756, MAE=9.872) followed by GBM, XGBoost, NNET, RF, CBoost and ENET. Simpler algorithms such as PLS, RR perform significantly worse, while the large number of predictors (620) appeared unsuitable for the OLS algorithm (RMSE=87.413). However, the overall performance of the models of higher complexity show only small, mostly insignificant improvements.

Table 4. The results of 10-fold CV on the training set using multi-temporal S-2 images

10 fold CV training set - Sentinel 2 multitemporal (S2 2018-07-25; S2 2018-08-01; S2 2018-08-29; S2 2018-09-28)				
model	**RMSE**	**R^2**	**MAE**	**Tuning parameters**
Multiple regression (Ordinary Least Squares) - OLS	87.413	0.593	14.458	
Partial Least Squares - PLS	15.020	0.650	10.770	ncomp = 10
Ridge Regression - RR	41.520	0.611	11.890	lambda = 0.1
Elastic Net - ENET	14.360	0.669	10.543	fraction = 0.2 lambda = 0.01
Model Averaged Neural Network - NNET	14.230	0.680	10.520	size = 11 decay = 0.1
Support Vector Machines with Radial Basis Function Kernel - SVM	13.756	0.697	9.872	sigma = 0.001703831 C = 2
Random Forest - RF	14.265	0.673	10.732	mtry = 213
Stochastic Gradient Boosting - GBM	13.952	0.685	10.369	n.trees = 910 interaction.depth = 7

Preprints (www.preprints.org) | NOT PEER-REVIEWED | Posted: 2 November 2020 doi:10.20944/preprints202011.0030.v1

				shrinkage = 0.01 n.minobsinnode = 30
Extreeme Gradient Boosting - XGBoost	13.991	0.683	10.348	nrounds=650 max_depth=4 eta=0.05
Catboost - Cboost	14.195	0.676	10.460	depth=6 learning_rate=0.1 leaf_reg=0.001 rsm=0.95

Validation of the models on the spatially independent test data overall show much worse results for all of the compared models. This is especially evident from the validation results of models based on the single S-2 image, presented in Table 5. The obtained validation metrics, in particular R^2, which range from 0.380 for SVM to 0.420 for RR and ENET are significantly lower than the results obtained in the training set. With the addition of the multi-temporal S-2 data, there was only a slight improvement in the model performances as shown in Table 6. The highest R^2 value, 0.445 was obtained by the ENET model, followed by other algorithms: CBoost (R^2=0.411) and GBM, RF, RR (R^2=0.440). These results emphasize the problem of spatial extrapolation of the model results or the suitability of the model for the prediction out of the training areas which is a very common problem in spatial analysis. Furthermore, in the case of extrapolation, the suitability of the simpler, robust, linear regularization algorithms such as ENET and RR is equal or slightly better that the suitability of the complex ensemble algorithms which show better realization only on the training data due to the probable overfitting.

Table 5. Model validation on the testing set: a single S-2 image (S2 2018-07-25)

Test set - Single Sentinel-2 image (S2 2018-07-25)			
model	**RMSE**	**R^2**	**MAE**
Multiple regression (Ordinary Least Squares) - OLS	15.264	0.406	11.655
Partial Least Squares - PLS	15.220	0.410	11.450
Ridge Regression - RR	15.110	0.420	11.230
Elastic Net - ENET	15.090	0.420	11.190
Model Averaged Neural Network - NNET	15.360	0.410	11.090
Support Vector Machines with Radial Basis Function Kernel - SVM	16.110	0.380	11.390
Random Forest - RF	15.290	0.410	11.240
Stochastic Gradient Boosting - GBM	15.580	0.400	11.150
Extreeme Gradient Boosting - XGBoost	15.645	0.387	11.233
Catboost - Cboost	15.488	0.403	11.171

 doi:10.20944/preprints202011.0030.v1

Table 6. Model validation on the testing set: multi-temporal S-2 images

Test set - Sentinel-2 multitemporal (S2 2018-07-25; S2 2018-08-01; S2 2018-08-29; S2 2018-09-28)			
model	**RMSE**	**R^2**	**MAE**
Multiple regression (Ordinary Least Squares) - OLS	15.264	0.406	11.655
Partial Least Squares - PLS	15.303	0.425	11.190
Ridge Regression - RR	15.359	0.440	11.140
Elastic Net - ENET	14.999	0.445	10.916
Model Averaged Neural Network - NNET	15.846	0.402	11.447
Support Vector Machines with Radial Basis Function Kernel - SVM	16.020	0.410	11.240
Random Forest - RF	14.900	0.440	10.935
Stochastic Gradient Boosting - GBM	14.940	0.440	10.730
Extreeme Gradient Boosting - XGBoost	15.102	0.428	10.874
Catboost - Cboost	14.951	0.441	10.793

3.3. The importance of satellite indices in prediction

Inferences about the contribution of particular satellite indices in the COP prediction are usually not the main goal in predictive modelling. However, for the purpose of simplifying the building process, in particular retrieval and pre-processing of the huge number of S-2 variables in eventual future similar studies, it is recommended to focus only on the group of the most valuable indices or features that significantly contribute to models. The common drawback of highly flexible modelling techniques such as neural networks, SVM, random forest and boosting is the lack of interpretability of the model in terms of inferences about the input variables. The important advantage of the R Caret framework is in its capability of quantification of the variable importance in various models. The variable importance is commonly estimated from the reduction in squared error due to each predictor. In ensembles, improvement values for each predictor are averaged across the entire ensemble to yield an overall importance value. The scores of the variable importance estimation for the best performing models on the multi-temporal set in this study are provided in Table 7.

Preprints (www.preprints.org) | NOT PEER-REVIEWED | Posted: 2 November 2020 doi:10.20944/preprints202011.0030.v1

Table 7. Variable importance scores for the top 20 satellite indices and related models. The S-2 columns refer to the positioning of the index variable in the multi-temporal set (I = 2018.07.25., II = 2018.08.01., III = 2018.08.29., IV = 2018.09.28.)

CBoost	S-2	Score	GBM	S-2	Score	XGBoost	S-2	Score
IPVI	I	100.00	CI	I	100.00	CI	I	100.00
NDTI	I	92.57	ARVI	I	36.53	ARVI	I	33.58
TNDVI	I	75.02	NDI45	III	32.07	IPVI	I	33.48
NDI45	IV	71.79	PSSRA	I	29.16	NDI45	III	19.74
NDI45	II	54.44	NDI45	II	26.5	PSSRA	II	13.47
NDTI	II	49.79	IPVI	I	22.65	NDI45	I	11.85
NDVI	IV	41.68	NDI45	IV	16.43	NDI45	IV	11.73
MCARI	I	40.58	CI	II	15.6	CI	II	10.79
ARVI	I	37.70	NDI45	I	15.02	IPVI	IV	5.63
RI	II	36.04	CI	IV	10.75	CI	IV	5.61
TNDVI	IV	34.42	IPVI	IV	7.27	NDI45	I	5.50
NDWI2	IV	32.80	ARVI	II	7.22	RI	II	4.62
CI	II	32.24	RI	II	7.08	MCARI	IV	4.18
PSSRA	I	31.53	PSSRA	II	6.04	MCARI	I	3.8
NDTI	IV	30.57	CI	III	5.99	ARVI	II	3.48
NDTI	III	29.08	MCARI	IV	5.65	CI	III	3.24
GLCM_VAR_B1	IV	28.21	MCARI	I	4.66	GLCM_VAR_B1	IV	2.54
ARVI	IV	27.97	PSSRA	II	4.61	ARVI	IV	2.46
CI	III	27.32	NDWI2	IV	4.08	NDWI2	IV	2.46
NDVI	I	26.11	ARVI	IV	3.64	PSSRA	II	1.78

ENET	S-2	Score	RF	S-2	Score	SVM	S-2	Score
ARVI	I	100	NDI45	IV	100	ARVI	I	100
TNDVI	I	98.85	ARVI	I	80.22	TNDVI	I	98.85
IPVI	I	98.85	MCARI	IV	79.45	IPVI	I	98.85
NDVI	I	98.85	RI	II	75.48	NDVI	I	98.85
RVI	IV	98.45	IPVI	IV	73	RVI	IV	98.45
RVI	I	98.45	PSSRA	I	71.2	RVI	I	98.45
ARVI	II	97.85	MCARI	I	69.72	ARVI	II	97.85
CI	I	97.73	CI	IV	69.61	NDTI	I	97.73
NDTI	I	97.73	CI	II	65.47	CI	I	97.73
PSSRA	I	97.46	CI	I	65.11	PSSRA	I	97.46
CI	II	96.73	NDVI	IV	63.8	NDTI	II	96.73
NDTI	II	96.73	NDTI	I	63.28	CI	II	96.73
IPVI	II	96.4	TNDVI	IV	62.23	IPVI	II	96.4
NDVI	II	96.4	NDTI	IV	59.98	NDVI	II	96.4
TNDVI	II	96.4	RVI	IV	59.08	TNDVI	II	96.4
PSSRA	II	96.28	NDTI	II	57.78	PSSRA	II	96.28
RVI	II	95.78	RVI	I	56.28	RVI	II	95.78

Preprints (www.preprints.org) | NOT PEER-REVIEWED | Posted: 2 November 2020 doi:10.20944/preprints202011.0030.v1

PSSRA	III	93.33	ARVI	IV	55.73	PSSRA	III	93.33
ARVI	III	92.24	NDVI	I	55.57	ARVI	IV	92.24
NDVI	III	91.45	TNDVI	I	54.88	NDVI	IV	91.45

The importance profile of provided scores in Table 7 provides some clues about how models incorporate into the data. GBM and XGBoost have a very steep slope of declining scores from top to bottom which is the usual for boosting algorithms. This is due to the fact that trees from boosting are dependent on each other - they have correlated structures as the method follows by the gradient. As a result, many of the same predictors are selected across the trees, increasing their contribution to the importance metric. The RF algorithm relies on the decorrelation of trees and the selection of a random number of variables at each tree node and therefore it has slower decline of scores. What could be distinguished among the models is the order of incorporating indices from the multi-temporal S-2 set across the importance profile. ENET (and also RR) gradually incorporates the most dominant predictors following the chronology of the multi-temporal S-2 set; first incorporating variables from the first S-2 image, then second and third (with the exception of rvi index from image four). Incorporation of the most dominant variables from the images in chronological order is probably the learning principle of regularization algorithm. It slides from image to image, repeatedly incorporates the most significant predictors that reduces SSE and shrinks or penalizes the others. What is also evident is that the ENET model relies only on the first three images in the multi-temporal set and the predictive information from the last set is probably redundant for the model construction. RF algorithm behaves quite oppositely to the ENET algorithm in that it alternately incorporates variables from the first, then fourth and second S-2 image without some discernible pattern.

Given the spectral indices used, there are also certain peculiarities amongst the models. In most cases, particular vegetation and soil radiometric indices play a dominant role. From the vegetation indices, the most significant are ARVI, IPVI, NDI45, PSSRA AND MCARI, of soil radiometric indices CI and RI and of water radiometric indices NDTI. Of the textural features, only GLCM_variance appears on channel B1 on the last S-2 set. It is also important to note that boosting techniques (GBM, XGBoost) first discriminate sites according to reflectance from the bare soil (CI index) and then from vegetation, unlike other models that build first on reflectance from the vegetation surface.

3.4. Final model building and COP map production

Based on the results of training and validation, the ENET algorithm was chosen to create the final model. The main reasons for choosing the ENET model were: (I) simplicity of the algorithm, (II) robustness, best validation results on the test set, (III) one of the shortest computing time amongst all models, (IV) requires smallest number of S-2 images (three) in the multi-temporal set compared to other methods. The final model is produced using all 8222 samples from the training and validation sets, and all predictors from the S-2 multi-temporal set, 620 in total. The validation metrics of the final ENET model was: RMSE=14.427, R^2=0.603 and MAE=10.821. The model was then used for the prediction of COP over the whole FMU Litorić. Due to the use of regression settings for the prediction of percentages on the interval between 0 and 100%, the final model also contained protruding predictions that were beyond this interval. In such cases, negative values were simply constrained to 0 and values above to the upper limit of 100. The final result of the whole modelling process, a map of COP percentage for FMU Litorić is presented in Figure 5. The precision of the produced map can be best perceived by the visual examination of individual details, such as presented in Figure 6 which shows a mixed segment with alternating forest cover and clearings.

Preprints (www.preprints.org) | NOT PEER-REVIEWED | Posted: 2 November 2020 doi:10.20944/preprints202011.0030.v1

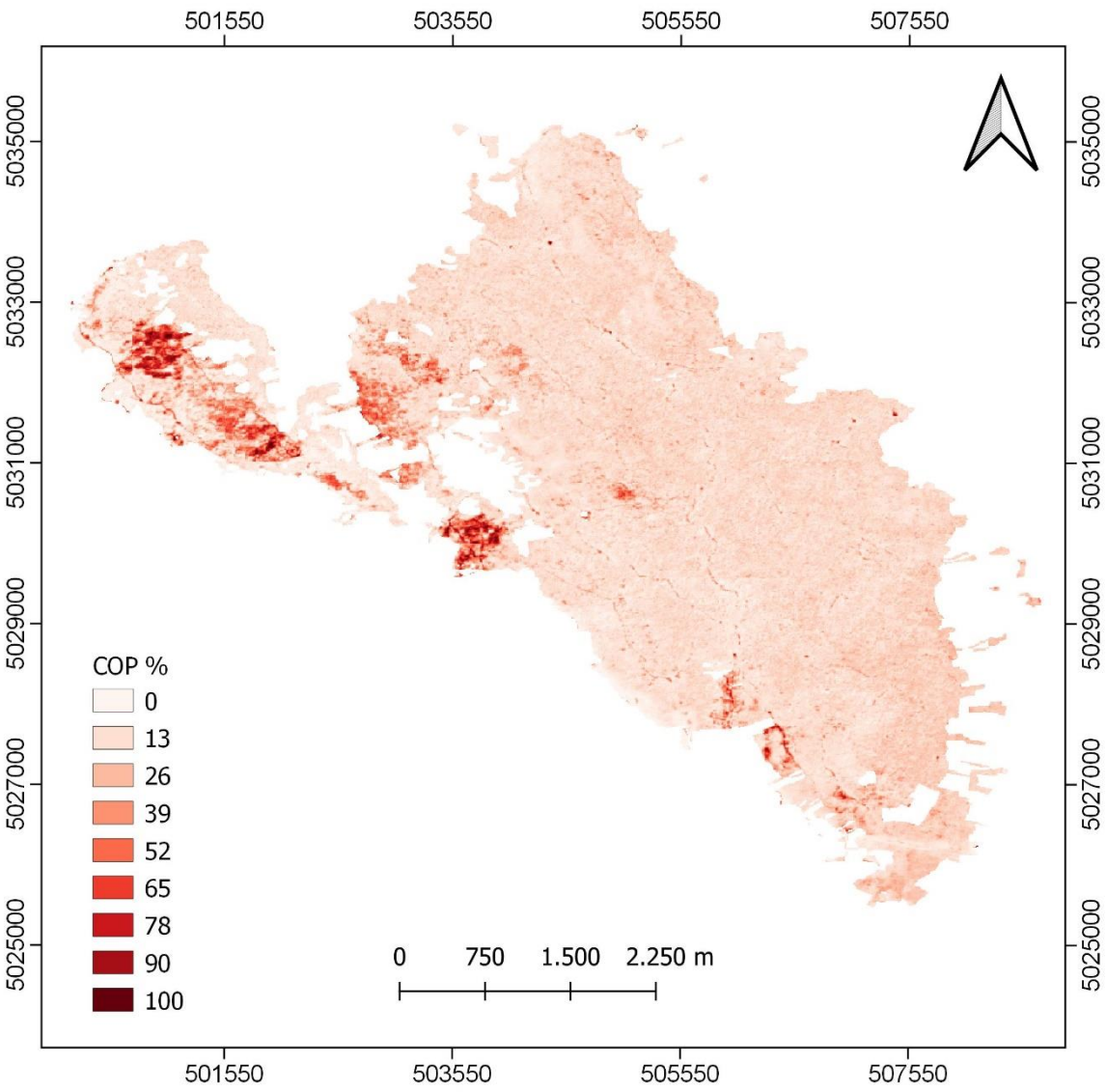

Figure 5. The final map of Canopy Openings Percentage for FMU Litorić

Preprints (www.preprints.org) | NOT PEER-REVIEWED | Posted: 2 November 2020 doi:10.20944/preprints202011.0030.v1

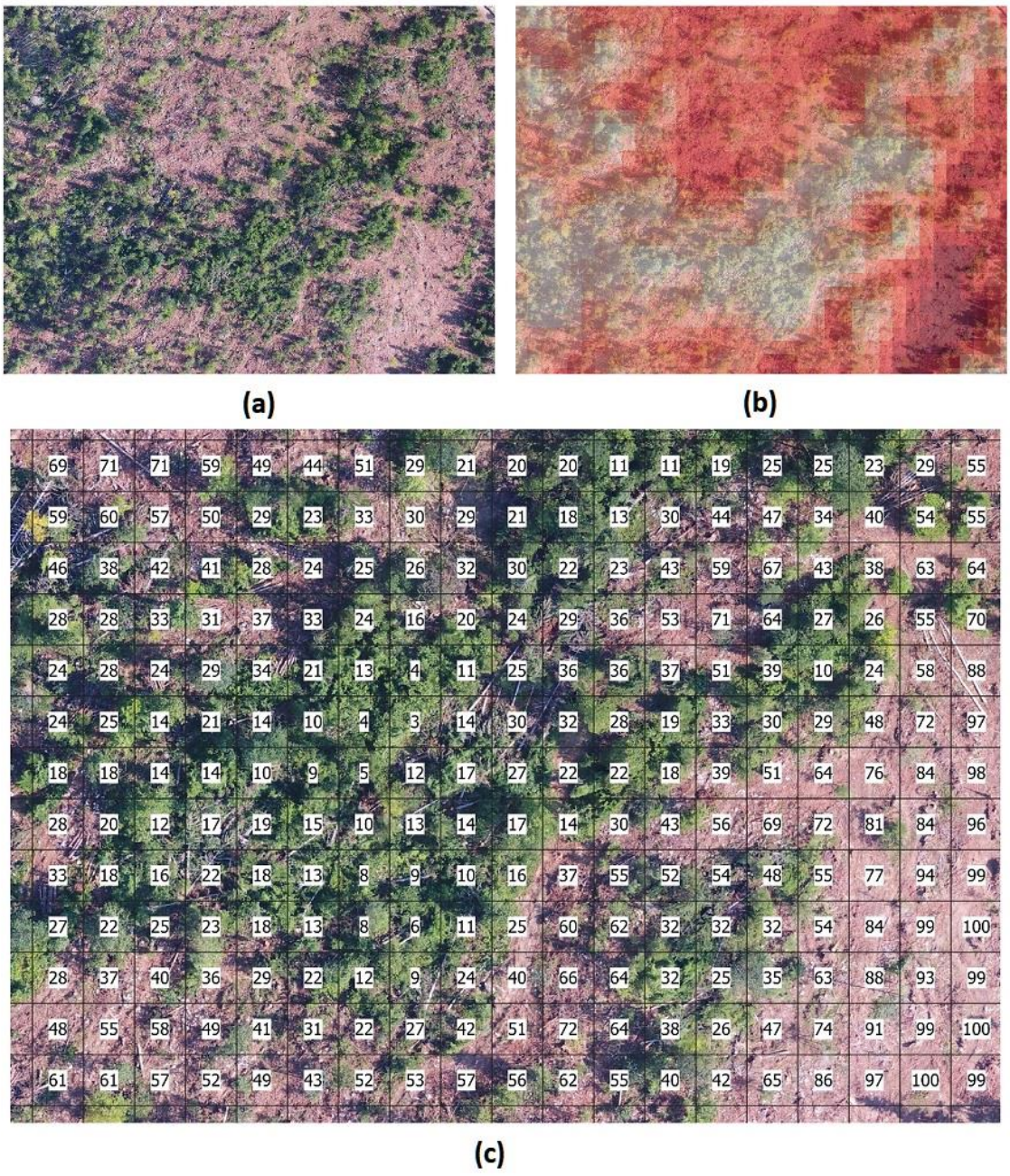

Figure 6. Representation of the map precision. **(a)** Detail of the area obtain by UAV image; **(b)** The same detail with overlayed COP map including marked areas in red that indicate disturbances of the canopy; **(c)** Precision of the map can be also perceived from the labels that display COP values in percentages across S-2 polygon grid

3.5. Analysis of residuals and observed shortcomings of the model

The relationship of observed vs predicted values from the final ENET model and the distribution of the residuals is presented in Figure 7.

Preprints (www.preprints.org) | NOT PEER-REVIEWED | Posted: 2 November 2020 doi:10.20944/preprints202011.0030.v1

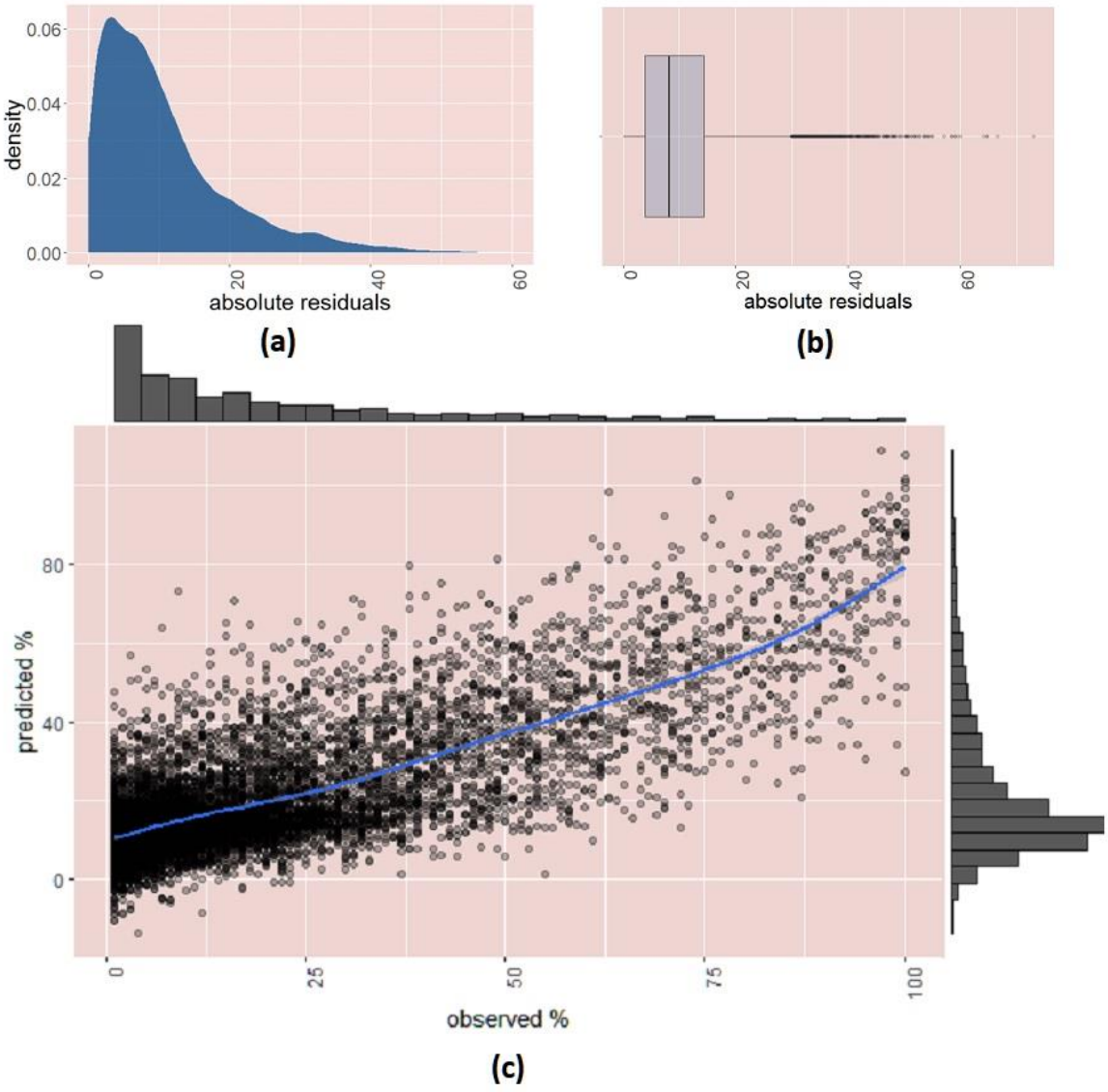

Figure 7. Assessment of the final model residuals. **(a)** Density plot of absolute residuals of the ENET model; **(b)** Boxplot of absolute residuals (median value = 8.2%); **(c)** Scatterplot of the observed vs. predicted values with distribution histograms

The model residuals are mainly spatially randomly distributed. In addition, we tried to explain some observed shortcomings of the model with respect to the limited degree of explanation of the variance of response (max R^2 of 0.697 in the training set and 0.603 in a final set). This was performed first by gaining insight into spatial patterns of observations with extreme positive and negative residual values and then with further visual examination of the potential reasons of these discrepancies on UAV images. One such case is presented on Figure 8 which shows two larger clearings within the forest on which the trees were completely absent. The clearing on the left side of the image contains a group of observations with positive residuals (model over estimation), while the clearing on right contains the group of negative residuals (model under estimation).

Preprints (www.preprints.org) | NOT PEER-REVIEWED | Posted: 2 November 2020 doi:10.20944/preprints202011.0030.v1

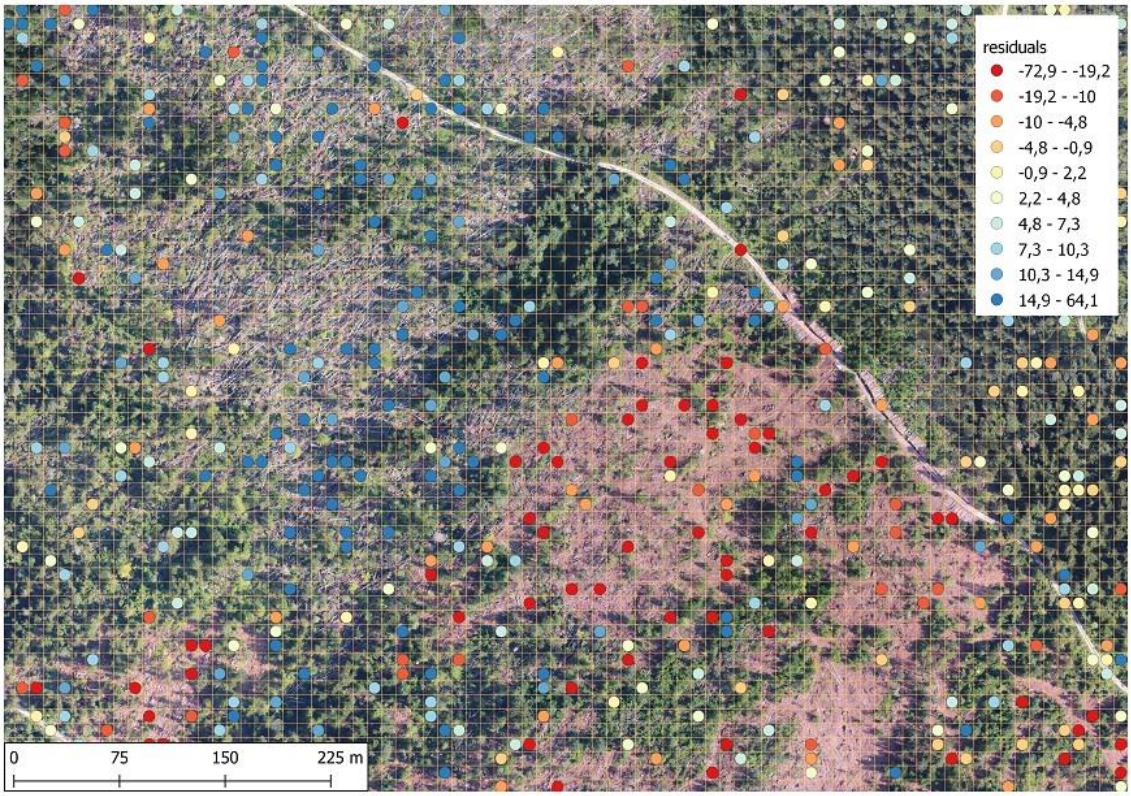

(a)

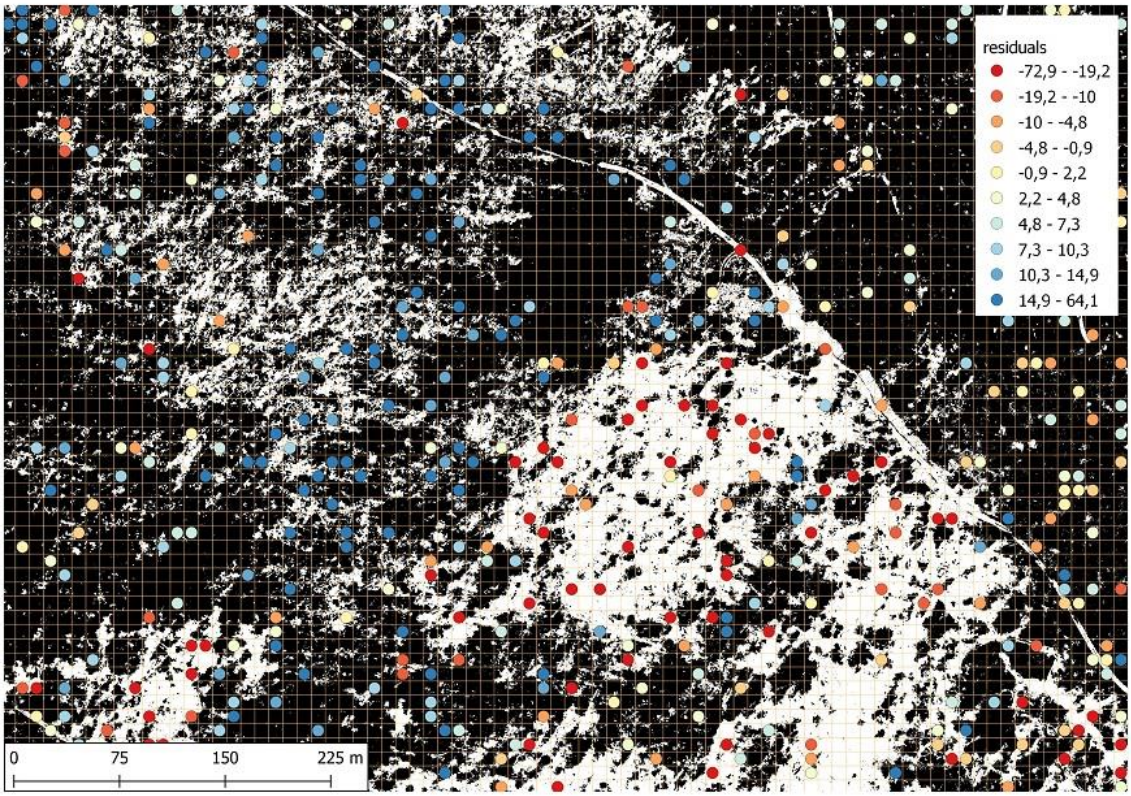

(b)

Figure 8. Representation of two cases of model discrepancies. **(a)** Contrasting areas of COP overestimation (blue points) and underestimation (red points); **(b)** The same forest segments with the UAV mask overlay with visible dissimilarity in abundance of open areas marked in white

Preprints (www.preprints.org) | NOT PEER-REVIEWED | Posted: 2 November 2020 doi:10.20944/preprints202011.0030.v1

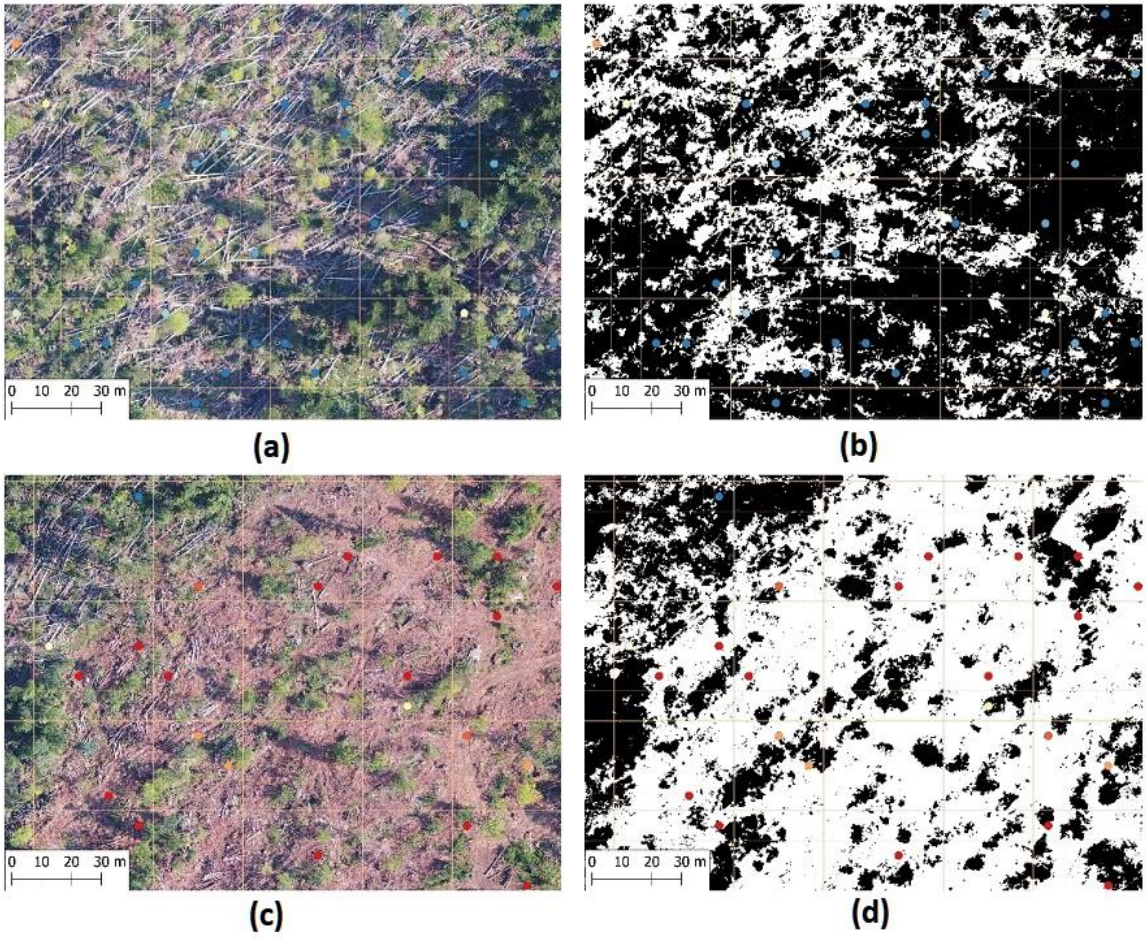

Figure 9. Deeper insight into two contrasting areas. (a) An area with fallen trees after a windstorm; (b) Comparative UAV mask that overestimates real forest cover; (c) Forest clearing with removed logs and noticeable bare ground with distinguishable soil color; (d) Comparative UAV mask of the forest clearing with scarce canopy cover

A deeper insight into the above locations reveals the difference in the surface cover. Namely, in the image on the left, the fallen trees, as a result of the recent wind break in the area of FMU Litorić, are noticeable, while in the image on the right, the trees have been completely cleared and the bare soil surface comes to expression. Fallen trees, somewhere still with a green canopy, as well as the shadows of the forest edge, are affected by the process of automatic production of the UAV forest mask, which in such cases shows a much lower COP percentage than in reality. The ENET model in such cases provides somewhat realistic COP values that are much higher than the UAV mask. In the figure on the right it is the opposite: on bare clearings the ENET model estimates significantly lower values than in the reality what causes negative residuals.

Another case of discrepancy was observed on locations where damaged trees with a higher degree of crown discoloration occurred. These trees that still form a complete canopy cover are falsely recognized as the open areas in the constructed UAV RGB forest mask (Figure 10). This can cause an overestimation of the COP prediction that is not realistic.

Preprints (www.preprints.org) | NOT PEER-REVIEWED | Posted: 2 November 2020 doi:10.20944/preprints202011.0030.v1

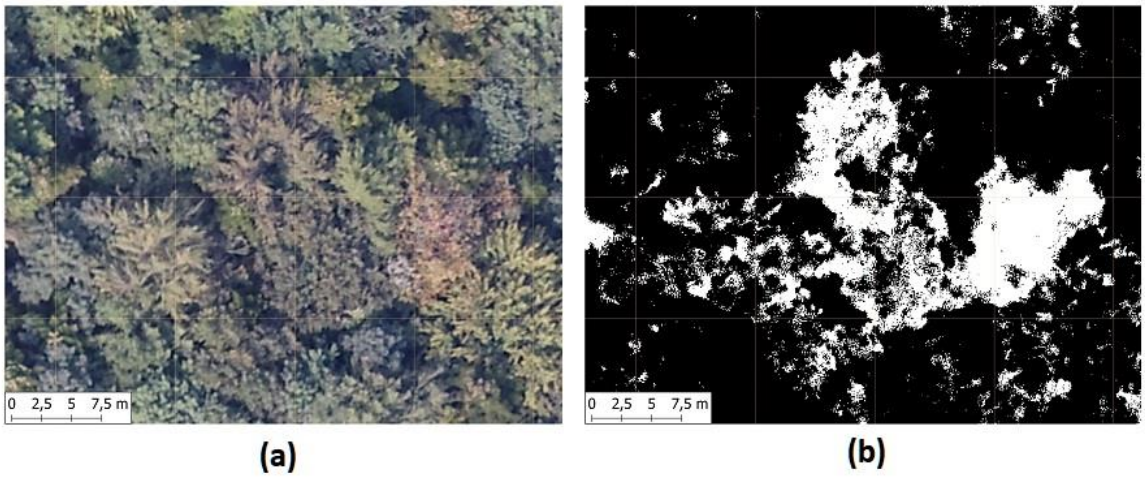

Figure 10. The example of false canopy gap creation from UAV RGB images over the damaged trees with crown discoloration. **(a)** UAV image segment of trees with the damaged canopy; **(b)** Related UAV mask with false open spaces presented in white.

4. Discussion

From the presented results of this research, the suitability of the combined method of COP estimation using UAV and Sentinel 2 images, intended for precise rapid mapping of COP on a large FMU scale, was demonstrated. As the main purpose of the presented approach is applicability in operational forest management or silvicultural decision-making processes, the method has certain trade-offs that resulted in a somewhat weaker overall prediction accuracy, at the expense of the promptness of the required data acquisition and the short time required for the final product manufacturing, which is usually one of the main requirements from the end-users in operational forestry for this kind of the EO product (e.g. when assessing large scale calamity caused by windthrows, ice breaks, etc.). The applied approach relies entirely on information from remote sensors in different image resolutions that allow both a detailed overview of ground truth data and wall-to-wall mapping for the entire FMU (3000-6000 hectares).

For the integration of different sensors, UAV and Sentinel-2, the predictive modelling approach was applied, which consisted of features engineering, the creation of training and validation sets of data, training of various algorithms using resampling techniques, validation of models on the test set, model selection, construction of the final model and prediction of the new samples. The model building process brought about the improvement of predictive performance on the training set in successive steps; (I) the highest R^2 of the single feature (derived satellite index) using simple linear regression was up to 0.57, (II) the highest R^2 using multiple features obtained from the single date, S-2 image and the best ML algorithm was 0.624, and (III) the highest R^2 on the multi-temporal set of four consecutive S-2 images, using the best ML algorithm reached 0.697.

From the wider range of satellite indices or features examined in this study, several of them exhibited superior properties in differentiating the COP gradient and were therefore incorporated as the main foundation in the majority of ML models. NDVI (Normalized Difference Vegetation Index), which most often represents the core index for determining variations in the structure of vegetation cover, did not prove to be the primary choice of ML algorithms examined in this research. They instead, as a primary choice, selected indices that are closely based on NDVI but with enhanced properties in certain segments. ARVI (Atmospherically Resistant Vegetation Index) like NDVI, is also based on the normalized difference between near-infrared and the red channel, but it corrects the atmospheric effect on the red channel by using the difference in the radiance between the blue and the red band. It has a similar dynamic range to NDVI but, on average, is four times less sensitive to

atmospheric effects. IPVI (Infrared Percentage Vegetation Index) is functionally equivalent to NDVI with the only difference that it includes infrared and red factor into the NDVI equation which results in simplification of the calculation process. The NDI45 (Normalize Difference Index) algorithm uses the same relations and bands but is more linear and usually less saturated at higher values than the NDVI. In addition to the above indices based on the improved NDVI principle, simple ratio indices that are sensitive to variations in chlorophyll concentrations in canopies have also been shown to be the dominant choice for ML algorithms. PSSRa (Pigment Specific Simple Ratio, or chlorophyll index), consists of a simple ratio of the near infra-red and red band. It belongs to narrow-band pigment indices that have the strongest and most linear relationship with canopy concentration per unit area of Chlorophyll a, Chlorophyll b, and carotenoids. MCARI (Modified Chlorophyll Absorption Ratio Index) is the ratio of differences in bands in the visible spectra (red, green, blue), responsive to chlorophyll variation, and ground reflectance. In addition to the mentioned vegetation radiometric indices, a few ML algorithms (GBM and XGBoost), as a first source, use a CI (Color Index) which belongs to the group of soil radiometric indices. CI was primarily developed to differentiate soils in the field, and in this study, it probably had the best properties to differentiate areas with bare soil within significantly disturbed canopy cower caused by recent windthrows. In most cases, it gives complementary information with the NDVI. RI (The Redness Index), like CI, also enables identifying the areas with bare soil, which in the FMU Litorić has a commonly reddish hue, characteristic for soils developed on hard limestone. Of the other used indices, of greater importance is the NDTI (Normalized Difference Turbidity Index) which belongs to the Water radiometric group of indices commonly used for the measurement of water turbidity or water clarity. Since the NDTI algorithm is color sensitive, its structure very similar to the CI algorithm, its representation in the models is complementary to the CI and RI indices.

The use of a multitemporal set of S-2 data, compared to information from the single S-2 image, contributed most significantly to an increase in the prediction results compared to all other examined means of prediction improvement. The highest achieved R^2 using 10-fold CV on the training set with data from a single S-2 image from 25.07.2018, which was closest to the UAV image acquisition, was 0.624. However, by including variables from the multi-temporal set, a significant increase in the explained COP variance from the multitemporal predictors was achieved (R^2 of 0.697). On the other hand, the use of a multi-temporal set led to an only slight improvement in RMSE (13.756) compared to single date variables (15.148) which ultimately makes a difference of only 1.3% of COP. The advantages of using a multi-temporal set of Sentinel 2 images vs a single image for the discrimination of the forest cover are in accordance with recently published results [56, 57]. The most likely reason for the enhanced results of the multi-temporal set is that, although the S-2 images were obtained within a short time interval (approx. two months), they were able to discern certain variations in phenology that are very significant for discriminating small changes in the forest cover structure. According to the results [57], classifications made using multi-temporal Sentinel 2 imagery of two contrasting seasons (spring and autumn) were the most accurate, while classifications based on the single-season spring images were the second most accurate. Classifications made using other combinations of seasons and feature types varied but yielded significantly lower accuracy. Incorporation of the Sentinel-2 image from the early spring aspect could most probably improve the COP prediction, but at the risk of loss of up-to-date insight into the current situation of the forest cover which is often crucial for operational silvicultural decisions.

The addition of ML models with varying degrees of complexity was one of the options in which an improvement in COP prediction was sought. The included ML algorithms on the single temporal S-2 training set with 10-fold CV only partially contributed to improved prediction. Compared to the basic OLS algorithm (RMSE = 15.684; R^2 = 0.603), the best XGBoost model (RMSE = 15.148; R^2 = 0.624) only slightly improved the prediction results (a decrease in RMSE of 0.536 and an increase in R^2 of 0.021). Although they showed a very small improvement of model metrics, a few ML algorithms like SVM, RF, GBM, XGBoost, CBoost showed somewhat better results, some algorithms like NNET underperformed while others like PLS, RR, and ENET had similar capabilities to OLS. A significant

 doi:10.20944/preprints202011.0030.v1

difference between the algorithms is noticeable on the multitemporal set between the basic OLS model (RMSE = 87.413; R^2 = 0.593) and the best SVM model (RMSE = 13.756; R^2 = 0.669). It should be noted that the basic, OLS algorithm, due to a large number of predictors, exhibits a problem with convergence and instability (high RMSE) and therefore it is unsuitable for the multi-temporal set.

One of the observed shortcomings of the method is that it is less suitable for extrapolation of COP outside the training area, i.e. lower prediction capabilities for COP mapping on the entire FMU area. This was obvious from the obtained metric from the spatially remote validation data set. The accuracy achieved on the test set is significantly lower than the accuracy obtained using 10-fold CV resampling on the training set. The best obtained RMSE and R^2 on a single S-2 image was 15.09 and 0.42, and on the multi-temporal set 14.900 and 0.445 respectively, which is significantly worse than the 10-fold CV from the training data. Also, more complex algorithms that were somewhat superior on the training set did not validate their advantages on the independent set. The benefit of using more complex ML algorithms is that they allow better adjustment to local conditions, while this advantage is lost in cases of extrapolation to new conditions out of the training area. In other words, complex ML algorithms generally overfit the local condition, while outside the training area they are comparable to simpler algorithms with greater robustness and generalization ability. These results indicate the inadequate sampling design of the ground-truth UAV data acquisition used for model creation and mapping of the whole FMU area in this study (sampling design of UAV locations were not considered preliminary). Poorer generalization capabilities of the model can be remedied by the acquisition of UAV ground-truth images from a larger number of smaller training areas across the FMU to incorporate the variety of conditions (stratified random sampling). The ML model constructed in this way, in addition to encompassing a wider range of diversity, would be used primarily for interpolation between the UAV survey locations rather than extrapolation as is the case in this study. Also, improved sampling design will enable much better performance of more complex ML models (RF and boosting) which are superb for the representation of conditions that are not beyond the range of data used for learning.

Precise and reliable delineation of the crown edge on UAV images presented one of the most important factors affecting the reliability of the model. The problems observed in this study stemmed from the limited capabilities of UAV images only in the visible RGB channel to accurately delineate the crown projection which was then used as reference values for COP modelling. According to our knowledge, research on the combined application of Sentinel-2 and UAV in similar, highly heterogeneous forest types such as mixed beech-fir forests has not been conducted so far, so a direct comparison of the obtained results is not possible. On the other hand, there are results in which a somewhat similar approach was used but in somewhat different forest conditions. In a similar study evaluating tree canopy cover [44] combined using Sentinel-2, Google Earth imagery, and ML methods, significantly better prediction was achieved (R^2 = 82.8%, RMSE = 8.68%) than in our study. However, higher accuracy of the assessment was obtained in the semi-arid Mediterranean silvopastoral system (Quercus ilex, Quercus suber) with sparse tree density and very contrasting bare soil with a distinctive color. In such conditions, it was possible to identify more clearly the crown boundary and produce a more accurate canopy mask layer which was the most likely reason for better assessment. In conditions of extremely complex canopy structure, as is the case with mixed beech fir forests, special attention should be paid when creating a canopy mask layer. Using images only from the visible part of the spectrum, relying solely on differences in colour between the canopy and ground, is often very unreliable due to the noises such as shadows at gap edges, groups of fallen trees after windthrows, etc. Discoloration and defoliation of individual, partially damaged trees, that are falsely rejected from the canopy mask using an automatic classification based only on color indices from the visible spectra, also represent an observed problem that probably affected the accuracy of the method.

 doi:10.20944/preprints202011.0030.v1

5. Conclusions

The development of new remote sensing methods such as UAV, new satellite sensors, and the increasing amount and availability of high quality and free of charge satellite data opens up new opportunities for improving decision making support in operational forest management. Satellite data has so far, through a large number of different examples, shown its distinct advantages for the detection of changes in forests, but most often in large areas and in coarser spatial resolution, where its robust nature comes to the fore. The use of satellite Earth Observations to obtain more accurate information of forest structure is most often hampered by the need for field collection of ground-truth information, that is required for better representation of forest characteristics, which is often very slow and costly. The so-called change detection methods that have been used most often to quantify differences caused by anthropogenic or natural changes in the forest structure provide only proxy, indirect representation inherited from the properties of used satellite index. On the other hand, the development of unmanned aerial vehicles and their applications in forest photogrammetry has made it possible to obtain very precise, near real time information on the forest structure in a very cost-efficient way. The high precision of photogrammetric UAV methods, due to the immense amount of information, and the limited flying range simultaneity represents constraints in the use of this method over the larger areas.

Sentinel-2 MSI, due to its advanced spectral characteristics, frequent revisit time and free of charge data availability, represents a highly usable system for various forestry applications. A prerequisite for more efficient use of Sentinel-2 in operational forestry, as well as other optical sensors, is the establishment of stochastic relationships between obtained reflectance in the various spectral bands on multi-spectral images as surrogate information from forests and common measurable stand parameters used in forest management.

In this study, we demonstrated the effectiveness but also emphasized detected weaknesses of the combined approach of assessment of one of the basic silvicultural parameters such as Canopy Openings Percentage (inverse of the Canopy Density Percentage) using a series of Sentinel-2 imagery and simple UAV RGB images. With the combined approach, the existing limitations of each sensor were annulled: a coarser spatial resolution of Sentinel 2 and a limited flying range of UAV. UAV imagery was used for precise representation of the canopy cover, Sentinel-2 as a scaling platform for transferring information from UAV to a wider spatial extent while the connection was established using an adequate ML algorithm. A fairly reliable estimate was obtained using a series of four consecutive Sentinel-2 images collected over a period of just over two months, which overlaps in time with the UAV recording. Using only one Sentinel-2 image to compare with UAV gave much poorer results. Also, for extrapolation of information over the whole FMU, slightly better final results were obtained by using a simpler and more robust linear regularization algorithm such as Elastic Net rather than other more complex and robust ML methods (Random Forest, Boosting, Support Vector Machines, Neural Networks).

Given the applicability in forestry, the method can be used for operational application, as support to silvicultural planning and decision making on an annual basis or any time when there is a need from users for up-to-date information of the state of the forest canopy such as in case of identified disturbances (windthrows, ice-breakage) but also for control of silvicultural or other activities (forest clearings, illegal loggings...). Although the approach has been demonstrated in very heterogeneous conditions such as those prevalent in the uneven-aged mixed beech-fir forest, it is possible to extend it to various other forest types and environmental conditions. Also, this approach is suitable for combining Sentinel-2 with other structural and functional parameters of stands that can be obtained directly from UAV sensors (LiDAR, multispectral, hyperspectral) in which there is a stochastic relationship with Sentinel-2 images.

Author Contributions: Conceptualization, I.P. and D.K.; methodology, I.P. and D.K.; validation, I.P. and D.K.; formal analysis, I.P., M.G. and A.N; writing—original draft preparation, I.P., M.G. and A.N.; writing—review and editing, I.P., M.G. and D.K.;

Funding: This research received no external funding

Acknowledgments: This research was undertaken as an additional activity within the Horizon 2020 project "My Sustainable Forest - Earth Observation services for silviculture".

Conflicts of Interest: The authors declare no conflict of interest.

References

1. Čater, M.; Diaci, J.; Roženbergar, D. Gap size and position influence variable response of Fagus sylvatica L. and Abies alba Mill. *For. Ecol. Manag.* **2014**, *325*, 128–135. http://dx.doi.org/10.1016/j.foreco.2014.04.001
2. Dobrowolska, D.; Veblen, T.T. Treefall-gap structure and regeneration in mixed Abies alba stands in central Poland *For. Ecol. Manag.* **2008**, *255*, 3469–3476. doi:10.1016/j.foreco.2008.02.025
3. Ugarković, D.; Tikvić, I.; Popić, K.; Malnar, J.; Stankić, I. Microclimate and natural regeneration of forest gaps as a consequence of silver fir (Abies alba Mill.) dieback. *J.For.* **2018**, 5-6, 235-245.
4. Muscolo, A.; Sidari, M.; Mercurio, R. Variations in soil chemical properties and microbial biomass in artificial gaps in silver fir stands. *Eur. J. For. Res.* **2007**, *126*, 59–65. DOI 10.1007/s10342-006-0145-3
5. Muscolo, A.; Sidari, M.; Bagnato, S.; Mallamaci, C.; Mercurio, R. Gap size effects on above and below-ground processes in a silver fir stand. *Eur. J. For. Res.* **2010**, *129*, 355-365. DOI 10.1007/s10342-009-0341-z
6. Albanesi, E.; Gugliotta, O.I.; Mercurio, I.; Mercurio, R. Effects of gap size and within-gap position on seedlings establishment in silver fir stands. *Forest@* **2005**, *2(4)*, 358-366.
7. Nagel, T.A.; Svoboda, M. Gap disturbance regime in an old-growth Fagus-Abies forest in the Dinaric Mountains, Bosnia-Hercegovina. *Can. J. For. Res.* **2008**, *38*, 2728-2737. doi:10.1139/X08-110
8. Nagel, T.A.; Svoboda, M.; Diaci, J. Regeneration patterns after intermediate wind disturbance in an old-growth Fagus-Abies forest in southeastern Slovenia. *For. Ecol. Manag.* **2006**, *226*, 268-278. doi:10.1016/j.foreco.2006.01.039
9. Diaci, J.; Pisek, R.; Boncina, A. Regeneration in experimental gaps of subalpine Picea abies forest in Slovenian Alps. *Eur. J. For. Res.* **2005**, *124*, 29-36. doi:10.1007/s10342-005-0057-7
10. Malcolm, D.C.; Mason, W.I.; Clarke, G.C. The transformation of conifer forests in Britain - regeneration, gap size and silvicultural systems. *For. Ecol. Manag.* **2001**, *151(1-3)*, 7-23. doi:10.1016/S0378-1127(00)00692-7
11. Navarro-Cerrillo, R.M.; Camarero, J.J.; Menzanedo, R.D.; Sánchez-Cuesta, R.; Quintanilla, J.L.; Sánchez, S. Regeneration of Abies pinsapo within gaps created by Heterobasidion annosuminduced tree mortality in southern Spain. *iForest* **2014**, *7*, 209-215. doi: 10.3832/ifor0961-007
12. Vilhar, U.; Roženbergar, D.; Simončić, P.; Diaci, J. Variation in irradiance, soil features and regeneration patterns in experimental forest canopy gaps. *Ann. For. Sci.* **2015**, *72*, 253-266. doi:10.1007/s13595-014-0424-y
13. Streit, K.; Wunder, K.; Brang, P. Slit-shaped gaps are a successful silvicultural technique to promote Picea abies regeneration in mountain forests of the Swiss Alps. *For. Ecol. Manag.* **2009**, *257*, 1902-1909 doi:10.1016/j.foreco.2008.12.018
14. Thurnher, C.; Klopf, M.; Hasenauer, H. Forest in Transition: A Harvesting Model for Uneven-aged Mixed Species Forest in Austria. *Forestry* **2011**, *84(5)*, 517-526. doi:10.1093/forestry/cpr021
15. Abdollahnejad, A.; Panagiotidis, D.; Surový, P. Forest canopy density assessment using different approaches – Review. *J. For. Sci.*, **2017**, *63(3)*, 106–115. doi:10.17221/110/2016-JFS
16. Paletto, A.; Tosi, V. Forest canopy cover and canopy closure: comparison of assessment techniques. *Eur. J. For. Res.* , **2009**, *128*, 265–272. doi: 10.1007/s10342-009-0262-x
17. Karhonen, L.; Karhonen, K.T.; Rautiainen, M.; Stenberg, P. Estimation of forest canopy cover: a Comparison of Field Measurement Techniques. *Silva Fenn.*, **2006**, *40(4)*, 577-588. DOI: 10.14214/sf.315
18. Arumäe, T.; Lang, M. Estimation of canopy cover in dense mixed-species forests using airborne lidar data. *Eur. J. Remote Sens.* **2017**, 51(1), 132–141. doi:10.1080/22797254.2017.1411169
19. Wu, X.; Shen, X.; Cao, L.; Wang, G.; Cao, F. Assessment of Individual Tree Detection and Canopy Cover Estimation using Unmanned Aerial Vehicle based Light Detection and Ranging (UAV-LiDAR) Data in Planted Forests. *Remote Sens.* **2019**, *11*, 908, 1-21. doi:10.3390/rs11080908

20. Deutcher, J.; Granica, K.; Steinegger, M.; Hirschmugl, M.; Perko, R.; Schardt, M. Updating Lidar-derived Crown Cover Density Products with Sentinel-2. IGARSS **2017**, 2867-2870. doi: 10.1109/IGARSS.2017.8127597
21. Karna K.Y.; Penman, T.D.; Aponte, C.; Bennett, L.T. Assessing Legacy Effects of Wildfires on the Crown Structure of Fire-Tolerant Eucalypt Trees Using Airborne LiDAR Data. *Remote Sens.* **2019**, *11*, 2433, 1-21. doi:10.3390/rs11202433
22. Huang, C.; Yang, L.; Wylie, B.; Homer, C. A strategy for estimating tree canopy density using Landsat 7 ETM+ and high resolution images over large areas. 2001. Proceedings of the Third International Conference on Geospatial Information in Agriculture and Forestry, Denver, Colorado, 5 - 7 November, **2001**.
23. Mon, M.S.; Mizoue, N.; Htun, N.Z.; Kajisa, T.; Yoshida, S. Estimating forest canopy density of tropical mixed deciduous vegetation using Landsat data; a comparison of three classification approaches. *Int. J. Remote Sens.* , **2012**, *33(4)*, 1042–1057.
24. Baynes, J. Assessing forest canopy density in a highly variable landscape using Landsat data and FCD Mapper software. *Aust. For.* , **2004**, 67(4), 247-253.
25. Joshi, C.; De Leeuw, J.; Skidmore, A.K.; van Duren, I.C.; van Oosten, H. Remote sensed estimation of forest canopy density: A comparison of the performance of four methods *Int. J. Appl. Earth Obs. Geoinf.*, **2006**, *8*, 84–95. doi:10.1016/j.jag.2005.08.004
26. Korhonen, L.; Hadi; Packalen, P.; Rautiainen, M. Comparison of Sentinel-2 and Landsat 8 in the estimation of boreal forest canopy cover and leaf area index. *Remote Sens. Environ.*, **2017**, *195*, 259-274. doi:10.1016/j.rse.2017.03.021
27. Mulatu, K.A.; Decuyper, M.; Brede B.; Kooistra L.; Reiche, J.; Mora, B.; Herold, M. Linking terrestrial LiDAR scanner and conventional forest structure measurements with multi-modal satellite data. *Forests*, **2019**, 10, 291. doi:10.3390/f10030291
28. Revill, A.; Florence, A.; MacArthur, A.; Hoad, S.; Rees, R.; Williams, M. Quantifying uncertainity and bridging the scaling ga pin the retrieval of leaf area indeks by coupling Sentinel-2 and UAV observations. *Remote Sens.* **2020**, 12, 1843. doi:10.3390/rs12111843
29. Copernicus Land Monitoring Service. Available online: https://land.copernicus.eu/ (assessed on 15.08.2020)
30. Sentinel 2 User Handbook, Rev 2; European Space Agency, 2015; pp. 64. Available online: https://sentinel.esa.int/documents/247904/685211/Sentinel-2_User_Handbook (assessed on 18.08.2020)
31. Lima, T.A.; Beuchle, R.; Langner, A.; Grecchi, R.C.; Griess, V.C.; Achard, F. Comparing Sentinel-2 MSI and Landsat 8 OLI imagery for monitoring selective logging in the Brazilian Amazon. *Remote Sens.* **2019**, *11*, 961; doi:10.3390/rs11080961
32. Masiliūnas, D. Evaluating the potential of Sentinel-2 and Landsat image time series for detecting selective logging in the Amazon. *Geo-information Science and Remote Sensing, Thesis Report GIRS-2017-27*, **2017**, p 54, Wageningen, The Netherlands.
33. Barton, I.; Király, G.; Czimber, K.; Hollaus, M.; Pfeifer, N Treefall gap mapping using Sentinel-2 images. *Forests*, **2017**, *8*, 426. doi:10.3390/f8110426
34. Šimić Milas, A.; Rupasinghe, P.; Balenović, I.; Grosevski, P. Assessment of Forest Damage in Croatia using Landsat-8 OLI Images. *SEEFOR*, **2015**, *6(2)*, 159-169. doi:/10.15177/seefor.15-14
35. Navarro, J.A.; Algeet, N.;Fernández-Landa, A.; Esteban, J.; Rodríguez-Noriega, P.; Guillén-Climent, M.L. Integration of UAV, Sentinel-1, and Sentinel-2 Data for Mangrove Plantation Aboveground Biomass Monitoring in Senegal. *Remote Sens.* **2019**, *11*, *77*. doi:10.3390/rs11010077
36. Pla, M.; Bota, G.; Duane, A.; Balagué, J.; Curcó, A.; Gutiérrez, R.; Brotons, L. Calibrating Sentinel-2 imagery with multispectral UAV derived information to quantify damages in Mediterranean rice crops caused by Western Swamphen (Porphyrio porphyrio). Drones, **2019**, *3*, 45. doi:10.3390/drones3020045
37. Castro, C.C.; Gómez, J.A.D.; Martin, J.D.; Sánchez, B.A.H.; Arango, J.L.C.; Tuya, F.A.C.; Diaz-Varela, R. An UAV and satellite multispectral data approach to monitor water quality in small reservoirs. *Remote. Sens.* **2020**, *12*, 1514. doi:10.3390/rs12091514
38. Copernicus Open Access Hub. Available online: https://scihub.copernicus.eu/ (assessed on 12.02.2020)
39. Xue, J.; Su, B. Significant Remote Sensing Vegetation Indices: A Review of Developments and Applications. *J. Sens.* **2017**, ID 1353691, 17. doi:10.1155/2017/1353691
40. Bannari, A.; Morin, D.; Bonn, F. A Review of vegetation indices. *Remote Sensing Reviews.* **1995**, Vol. 13, 95-120. doi:10.1080/02757259509532298

41. Silleos, N.G.; Alexandridis, T.K.; Gitas, I.Z.; Perakis, K.; Vegetation Indices: Advances Made in Biomass Estimation and Vegetation Monitoring in the Last 30 Years. *Geocarto International* **2006**, *21(4)*, 21-28.
42. Escadafal, R.; Girard, M.C.; Courault, D. Munsell soil color and soil reflectance in the visible spectral bands of landsat MSS and TM data. *Remote Sens. Environ.* **1989**, *27 (1)*, 37-46.
43. Djamai, N.;, Zhong, D.; Fernandes, R.; Zhou, F. Evaluation of Vegetation Biophysical variables Time Series Derived from Synthetic Sentinel-2 Images. *Remote Sens.* **2019**, 11, doi:10.3390/rs11131547
44. Godinho, S.; Guiomar, N.; Gil, A. Estimating tree canopy cover percentage in a mediterranean silvopastoral systems using Sentinel-2A imagery and the stochastic gradient boosting algorithm. Int. J. Remote Sens., **2018**, *39(14)*, 4640-4662. doi:10.1080/01431161.2017.1399480
45. Haralick, R.; Shanmugam, K.; Dinstein, I. Textural Features for Image Classification. *IEE Transactions on systems, man and cybernetics*, **1973,** *3(6)*, 610-621.
46. Wickham, H. Tidy data. Journal of statistical software. **2014**, *59(10), 1-23.*
47. Gašparović, M.; Seletković, A.; Berta, A.; Balenović, I. The evaluation of photogrammetry-based DSM from low-cost UAV by LiDAR-based DSM. *SEEFOR*, **2017**, *8(2)*, 117-125.
48. Gašparović, M., Zrinjski, M., Barković, Đ., & Radočaj, D. An automatic method for weed mapping in oat fields based on UAV imagery. *Comput Electron Agric.*, **2020**, *173*, 105385.
49. Mathieu, R.; Pouget, M.; Cervelle, B.; Escadafal, R. Relationships between satellite-based radiometric indices simulated using laboratory reflectance data and typic soil color of an arid environment. *Remote Sens. Environ.*, **1998**, *66(1)*, 17-28.
50. Madeira, J., Bedidi, A., Cervelle, B., Pouget, M., & Flay, N. Visible spectrometric indices of hematite (Hm) and goethite (Gt) content in lateritic soils: the application of a Thematic Mapper (TM) image for soil-mapping in Brasilia, Brazil. *Int. J. Remote Sens.*, **1997**, *18(13)*, 2835-2852.
51. Escadafal, R.; Huete, A. Etude des propriétés spectrales des sols arides appliquée à l'amélioration des indices de végétation obtenus par télédétection. *Comptes rendus de l'Académie des sciences. Série 2, Mécanique, Physique, Chimie, Sciences de l'univers, Sciences de la Terre*, **1991**, *312(11)*, 1385-1391.
52. Louhaichi, M.; Borman, M. M.; Johnson, D. E. Spatially located platform and aerial photography for documentation of grazing impacts on wheat. *Geocarto International*, **2001**, *16(1)*, 65-70.
53. Tucker, C. J. Red and photographic infrared linear combinations for monitoring vegetation. *Remote Sens Environ.*, **1979**, *8(2)*, 127-150.
54. Gitelson, A. A., Kaufman, Y. J., Stark, R., & Rundquist, D. Novel algorithms for remote estimation of vegetation fraction. *Remote Sens Environ.*, **2002**, *80(1)*, 76-87.
55. The Caret Package: Available online: http://topepo.github.io/caret/index.html (assessed on 18.05.2020)
56. Wittke, S.; Yu, X.; Karjalainen, M.; Hyyppä, J.; Puttonen, E. Comparison of two-dimensional multitemporal Sentinel-2 data with three dimensional remote sensing data sources for forest inventory parameter estimation over a boreal forest. *Int. J. Appl. Earth Obs. Geoinformation*, **2019**, *76*, 167–178. doi:10.1016/j.jag.2018.11.009
57. Macintyre, P.; van Niekerk, A.; Mucina, L. Efficacy of multi-season Sentinel-2 imagery for compositional vegetation classification. *Int. J. Appl. Earth. Obs. Geoinformation*, **2020**, *85*, 101980. doi:10.1016/j.jag.2019.101980